Journal of Intelligent Material Systems and Structures OnlineFirst, published on November 5, 2009 as doi:10.1177/1045389X09352814

Tailoring the Response Time of Shape Memory Alloy Wires through Active Cooling and Pre-stress

YONAS TADESSE,* NICHOLAS THAYER AND SHASHANK PRIYA

Department of Mechanical Engineering, Center for Intelligent Material and Systems (CIMSS) Virginia Polytechnic Institute and State University, Blacksburg, VA 24061, USA

ABSTRACT: Application of shape memory alloy (SMA) actuators is limited to low frequencies due to slow cooling time especially in the embedded conditions where heat transfer rate is the controlling factor. In this study, we investigate various active cooling techniques and effect of pre-stress to improve the response time of two commercially available SMAs: Flexinol from Dynalloy Inc. and Biometal fiber from Toki Corporation. Flexinol and Biometal fiber of equal length and diameter were found to exhibit different actuation behavior under pre-stress. Time domain force response of SMA actuators was found to be dependent upon the applied pre-stress, heating rate, and amplitude of applied electrical stimulus. Compared to Biometal fibers, time domain response of Flexinol was found to decrease significantly with increasing pre-stress indicating the difference in transformation behavior. Fluid flow and heat sinking were found to be suitable methods for improving the response time by reducing the cooling cycle from 1.6 s to 0.30–0.45 s. This is a significant improvement in the actuation capability of SMAs.

Key Words: actuator, shape memory alloy, active cooling, pre-stress, response time.

INTRODUCTION

SHAPE memory effect is generally referred to the recovery of original shape from deformed shape with residual strain through thermal cycling. The superelastic behavior found in shape memory alloys (SMAs) is defined as the recovery of large strain by mechanical cycling under constant temperature (Otsuka and Wayman, 1999; Yan and Nei, 2003). Using the 3D diagram shown in Figure 1 the correlation between these two phenomenon can be explained. In a SMA wire, under normal atmospheric conditions, a pseudo-elastic deformation can be induced by applying stress, which is recoverable by thermal heat. The superelastic behavior in SMAs occurs at high temperature where the strain exhibits hysteresis with load (Shaw, 2000). SMAs have various advantages as compared to that of conventional actuators, namely (i) overall profile is low, (ii) high force to weight ratio, (iii) deploy simple current drive, and (iv) operation is silent. In spite of these advantages, SMAs have limited application due to their low operational frequency and narrow bandwidth. The bandwidth is limited due to the time required for heating and cooling of the actuators. The response time of SMA actuator is also dependent on preloading stress, loading condition and amplitude of activation potential. Table 1 compares SMA actuator with other low profile actuator technologies in terms of important performance indices. We have demonstrated working prototypes of robotic head utilizing various actuation technologies for both actuation and sensing (Tadesse et al., 2006) that includes servo motor-based actuation with piezoelectric sensing (Tadesse and Priya, 2008) and SMA actuation. In addition to humanoid faces, our interest in SMAs is for developing biomimetic unmanned undersea vehicles. Both of these applications require dynamic response in low frequency ranges (<10 Hz) with high force and low power consumption. Further, it is important to have high degree of linearity over large number of cycles. Comparing the actuation technologies listed in Table 1, SMAs have high force and strain in low frequency regime but low efficiency or high power consumption. Further, the time domain response of SMAs is slow. In order to overcome these problems we investigated the effect of pre-stress on the time domain response of SMAs and identified the role of pre-stress condition in enhancing the response time.

SMA actuators based on nickel and titanium (NiTi) are commercially available in wire forms. Two widely used SMA wires known as Flexinol (Dynalloy Inc., USA) and Biometal fiber (Toki Corporation, Japan) have been demonstrated in variety of applications. Biometal fiber is being experimented for applications in robotics, micro-gripper, artificial arm, and wing morphing. Implantable artificial myocardium has been proposed using Biometal fiber to mimic the natural ventricular contraction (Shiraishi et al., 2005).

*Author to whom correspondence should be addressed. E-mail: yonas@vt.edu
Figures 1–17 appears in color online: http://jim.sagepub.com

1045-389X/09/00 0001–22 $10.00/0 DOI: 10.1177/1045389X09352814

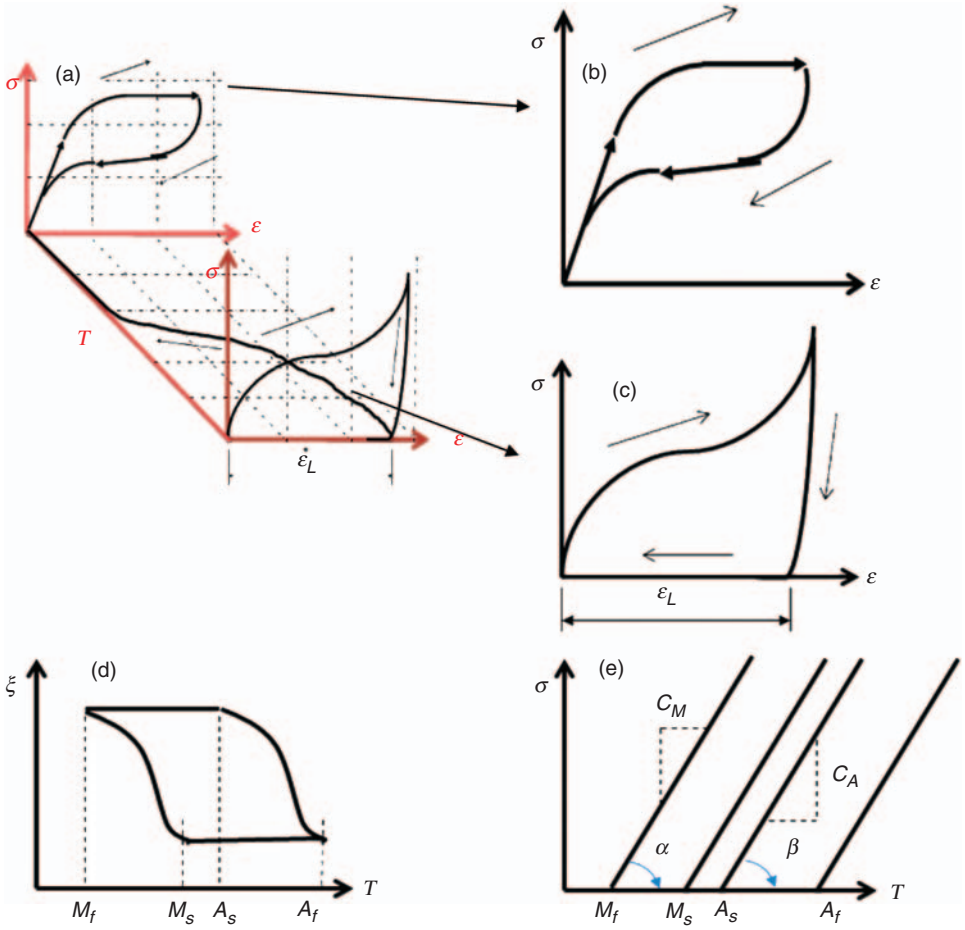

Figure 1. *Characteristics curves for SMAs: (a) 3D characteristic behavior (T-ε-σ), (b) superelastic behavior, (c) shape memory effect, (d) fraction of martensite as a function of temperature, and (e) stress vs transition temperature showing the four characteristic temperature, M_s, M_f, A_s, and A_f. The characteristic temperatures may be different for Flexinol and Biometal fiber.*

Biometal fiber has also been demonstrated as a variable damping isolator to enhance precision of optical equipments on-board satellites (Oh et al., 2005) and Jellyfish unmanned underwater vehicle (Villanueva et al., 2009). Flexinol has been demonstrated in various applications including robot-eye system (Choi et al., 2008), prosthetic hands (Loh et al., 2005a,b), and robotic manipulator (Ashrafiuon et al., 2006). An anti-glare rear-view mirror based on SMA actuation has been demonstrated by Luchetti et al. (2009) for automobile application where silicone elastomer coating was used to reduce the cooling time as well as thermal stress in SMA. Thus, both of these commercial SMAs are important actuator systems with potential in practical applications.

Prior studies on SMA motors or other applications indicate that SMA actuation has challenges in terms of achievable velocity (Pons et al., 1997). In order to overcome the problem of response time, Reynaerts and Van Brussel (1991) proposed the use of SMA coupled with fluid cooling system to realize torsional actuator. Bergamasco et al. (1989) have proposed SMA springs coupled with fluid cooling system for similar purpose and obtained a cutoff frequency of 2.0 Hz using a 0.5 mm diameter coiled wire. Russell and Gorbert (1995) proposed the use of a mobile sink that uses a friction clutch mechanism to cool a rotating lever arm. They determined that temperature feedback could help the cooling time by preventing the wire from overheating. Luo et al. (2000) implemented a series of Peltier modules to characterize the improvement in response time in SMA. Their results yielded a decrease in response time by 10 times, but it was still too slow to use in most robotic systems. Loh et al. (2005a,b) ran a SMA wire through a small metal tube filled with silicone grease that had a high thermal conductivity and reported a frequency response of 0.2 Hz but the power consumption was too high. Hunter et al. (1991) improved the response time of SMA by providing the wire a brief but large pulse of current. This improved the recovery time of the wire but displacement was less than a millimeter for each cycle, which may not be suitable for some robotic systems. Howe et al. (1995) have suggested pneumatic cooling for controlling a tactile display. They managed to reach a working frequency of 6–7 Hz through air cooling. All of these prior reported methods yielded some improvement but are not directly

Table 1. Comparison of SMA actuator with other low profile actuator technologies in terms of relevant performance indices.

Actuator type	Max. strain (%)	Max. pressure (MPa)	Max. energy density (J/cm^3)	Max. efficiency (%)	Specific density	Relative speed	E.g., Device or sample size	Drive (voltage/current)
1. Electrostrictive polymer Artificial muscle (Kornbluh et al., 1998)								
– Silicone	32	0.21	0.034	90	1	Fast	Thickness 1–4 μm	200 V
– Polyurethane	11	1.9	0.10	80	1	Fast		
– P(VDF-TrFE)	4	15	0.3	–	1.8	Fast		
2. Dielectric elastomer (Kornbluh et al., 2000)								
– Acrylic	215	7.2	3.4	60–80	1	Medium	– 3 mm diameter pump	–150 MV/m
– Silicon(CF 19-2186)	63	3.0	0.75	90	1	Fast	– 150 μm diaphragm	–190–300 V
3. Piezoelectric								
– Ceramic (PZT)	0.2	110	0.10	>90	7.7	Fast	120 × 27 × 0.3 beam	–1500/50
– Single crystal (PZN-PT)	1.7	131	1.0	>90	7.7	Fast		
– PVDF	0.1	4.8	0.0024	–	1.8	Fast		
– MFC (d_{33} mode) (Kornbluh et al., 2000; www.smart-materials.com)	0. 45	>40	–	–	–	Fast		
4. Shape memory alloy (NiTi) (Dynalloy Inc. (Available online at http://www.dynalloy.com.) Toki. Corp. (Available online at http://www.toki.co.jp.))	>5	>200	>5	<10	6.5	Slow	Wire diameter 25–500 μm commercially available	
5. Shape memory polymer (Polyurethane) (Kornbluh et al., 2000)	100	4	2	<10	1	Slow		<10
6. Electrochemomechanical								
– Conducting polymer (Madden et al., 2004)	2	7–34	23	<1	~1	Slow 13.8%/s[a]		<10
– TFSI-doped PPy (Hara et al., 2006)	37	≈1						
– Polyaniline (Kornbluh et al. 2000)								
7. Ionic polymer metal composite (IPMC) (Madden et al., 2004; Akle et al., 2006)	>2	≈15	0.005	2.9	–	3.3%/s	–30 × 3 × 0.21 mm^3 cantilever	<10 V
– Using cantilever effect (Baughman, 2005)	40							
8. Liquid crystal Elastomer (Madden et al., 2004)	45	0.45	0.056	<5	6–37%/s	0.45		1.25 MV/m
9. Magnetostrictive (Terfenol-D, Etrema Products) (Kornbluh et al., 2000)	0.2	70	0.025	60	9	Fast		
10. Natural muscle (skeletal muscle) (Kornbluh et al.,2000; Baughman, 2005)	>40	0.35	0.07	>35	1	Med		N/A

[a]High performance tubular actuator.

Table 2. Dimensions and actuation parameters of SMA wires as provided by commercial vendors.

Commercially available SMA actuators parameters	Flexinol (Dynalloy, Inc. Available online at http://www.toki.co.jp.)		Biometal fiber BMF100 (Toki Corp. Available online at http://www.dynalloy.com.)
	Sample 1	Sample 2	
Diameter	$D = 100\,\mu m$	$D = 127\,\mu m$	$D = 100\,\mu m$
Length	$L = 100\,mm$	$L = 100\,mm$	$L = 100\,mm$
Max. force	$F = 150\,gm$	$F = 230\,gm$	$F = 70\,gm$[a]
Recommended power	$P = 4.86\,W/m$	$P = 4.4\,W/m$	$P = 5.4\,W/m$
Current	$I = 180\,mA$	$I = 250\,mA$	$I = 200\,mA$
Voltage	$V = 27\,V/m$	$V = 17.6\,V/m$	$V = 27\,V/m$
Resistance	$R = 150\,\Omega/m$	$R = 70\,\Omega/m$	$R = 135\,\Omega/m$
Transformation temperature	90°C		70°C
Weight/Density	$W = 6.45\,gm/cm^3$		$W = 6.37\,gm/cm^3$
Strain	3–5%		4%
Specific heat	6–8 Cal/mol °C		6.1–8 Cal/mol °C
Life	–		$>10^6$ cycles
Category	Ni–Ti alloy		Ni–Ti alloy

[a]Practical force produced.

applicable towards using SMA in compact areas demanding large strain and force with minimum power consumption. There are several studies that describe methods for rapid heating of SMAs (Qiu et al., 2000), but our objective is to achieve low overall response time. These requirements are imposed by the application of SMAs in expressive humanoid face that is capable of displaying an array of emotions in real-time. Current design of humanoid head has an enclosed pocket of air in the skull, which becomes heated during the operation, causing the thermal response time to increase. Since the human face is capable of exhibiting motion up to 8 Hz, it is very important to decrease the response time of SMA by active cooling or pre-stressing to maintain the performance.

The relevant parameters for SMA actuators selected in this study are listed in Table 2. One of the clear physical difference between the two SMA actuators (Flexinol and Biometal) is their flexibility; Biometal fiber being more flexible than Flexinol. Other differences can be noticed in terms of maximum stress and transformation temperature. Two important parameters that should be compared for these actuators are blocking force and free displacement or strain. The blocking force is maximum force generated at zero stress whereas the free strain is maximum strain under no load condition. The operating point of the actuator is dependent on the loading experienced during application. As the loading is increased, response time of actuator will decrease. Thus an important parameter missing in Table 2 is variation of blocking force and strain with pre-stress. In robotic applications of SMAs, this is an extremely important data as the load changes can easily occur due to varying surrounding conditions. For example – SMAs used as artificial muscles in facial robotics may be exposed to varying stress magnitudes due to real-time interaction with user.

CONSTITUTIVE MODEL OF SMA

The actuation properties of SMAs can be explained by considering the thermomechanical constitutive theory. Several approaches have been proposed in literature and we mention the models relevant to our results in this manuscript. A 3D thermodynamic constitutive model has been developed by Boyd and Lagoudas (1994) based on thermodynamics. Tanaka et al. (1994) have presented phenomenological approach based on four-phase transformation. Patoor and Berveiller (1997) and Lubliner and Auricchio (1996) have modeled the behavior based on plasticity theory. All these models present general correlation between the parameters of SMA, namely stress, strain, and fraction of martensite as a function of temperature. Considering a 1D actuation of SMA, the thermomechanical response can be predicted by simultaneously solving the heat transfer equation and Hooke's law. Neglecting thermal expansion, the 1D governing equation for SMA actuator has been derived by Leo (2007) as:

$$\sigma - \sigma_0 = E(\varepsilon - \varepsilon_0) + \Omega(\xi - \xi^0), \tag{1}$$

where σ and σ_0 represent the stress and the pre-stress in the SMA actuator; E is the Young's modulus; ε and ε_0 are the current and initial strain; ξ and ξ^0 are the current and initial value of fraction of martensite with range between 0 and 1 ($\xi = 1$ for martensitic phase and $\xi = 0$ for austenitic phase); Ω is the transformation coefficient of material constant which can be determined from hysteresis SMA loop (as shown in Figure 1). The coefficient can be obtained from the residual strain and modulus of elasticity as: $\Omega = E\varepsilon_l$.

The fraction martensite equation as a function of temperature can be obtained from kinetic law. The characteristic curve for SMA actuators is shown in Figure 1(d) showing four transition temperatures;

M_s and M_f are the martensite start and finish temperature, and A_s and A_f are the austenite start and finish temperatures. Considering the austenite–martensite and martensite–austenite transformations as harmonic functions of cosines, the fraction of martensite can be expressed as (Leo, 2007):

$$\xi_{M-A} = 0.5\{\cos[a_A(T - A_s)] + 1\}, \tag{2a}$$

where $a_A = \pi/A_f - A_s$

$$\xi_{A-M} = 0.5\{\cos[a_M(T - M_f)] + 1\}, \tag{2b}$$

where $a_M = \pi/M_s - M_f$.

Above expressions are suitable for the case of zero applied stress. If pre-stress is applied on the SMA actuator, the transformation temperature changes and a modified form of Equation (2) should be utilized as follows:

$$\xi_{M-A} = 0.5\left\{\cos\left[a_A(T - A_s) - \frac{a_A}{C_A}\sigma\right] + 1\right\}, \tag{3a}$$

$$\xi_{A-M} = 0.5\left\{\cos\left[a_M(T - M_f) - \frac{a_M}{C_M}\sigma\right] + 1\right\}. \tag{3b}$$

Figure 1(e) illustrates the relationship between the transformation temperature and stress. The slope of stress and transformation temperature provides the value of C_A and C_M, which corresponds to the austenite and martensite, respectively. The rate form of Equations (1) and (3) is given as:

$$\dot{\sigma} = \dot{E}(\varepsilon - \varepsilon_0) + E(\dot{\varepsilon}) + \dot{\Omega}(\xi - \xi^0) + \Omega(\dot{\xi}), \tag{4}$$

$$\dot{\xi}_{M-A} = -0.5\left\{\sin\left[a_A(T - A_s) - \frac{a_A}{C_A}\sigma\right]\right\}\left\{a_A(\dot{T}) - \frac{a_A}{C_A}\dot{\sigma}\right\}, \tag{5a}$$

$$\dot{\xi}_{A-M} = -0.5\left\{\sin\left[a_M(T - M_f) - \frac{a_M}{C_M}\sigma\right]\right\}\left\{a_M(\dot{T}) - \frac{a_M}{C_M}\dot{\sigma}\right\}. \tag{5b}$$

The term $\dot{\sigma}$ is the force generated by SMA actuator, which is highly non-linear due to the presence of pre-stress term within the harmonic function for martensite fraction rate. Due to the coupled nature of these equations, it is expected that the relationship between force generation and pre-stress load are highly non-linear.

THERMAL MODEL OF SMA

Determination of a heat transfer coefficient provides insight into the phenomena associated with different types of active cooling techniques. The heat transfer coefficient of SMA wires can be obtained mathematically by assuming a lumped capacitance model. Lumped parameter model works on the assumption that the hot wire is suddenly submerged in an infinite medium with constant temperature. The wire is assumed to be thin enough that it has no internal thermal gradient. For these assumptions to be valid, the *Biot number* defined by Equation (6) has to be much less than 1.

$$Bi = \frac{hL_c}{k} \ll 1, \tag{6}$$

where Bi is the Biot number, h is the average heat transfer coefficient (W/m^2K), L_c is the characteristic length (m), and k is the thermal conductivity of SMA (W/mK). If Equation (6) is satisfied then the transient temperature can be obtained from lumped capacitance heat transfer equation (Incropera et al., 2007) and given by Equation (7) as:

$$\dot{T} = -\frac{hA}{\rho Vc}(T - T_\infty). \tag{7}$$

For constant convective heat transfer the solution is given by Equation (8):

$$T = T_\infty + (T_i - T_\infty)e^{-\lambda t}, \tag{8}$$

where $\lambda = A_s h/\rho vc$, ρ is the density, c is the heat capacity, v is the volume, A_s is the surface area, t is the time, T is the temperature of the wire, T_∞ is the ambient temperature, and T_i is the initial temperature of the wire. Note that Equation (8) is a simplistic equation, which can be used to study the heat transfer coefficient for active fluid cooling.

EXPERIMENTAL

Experimental Setup for Active Cooling

In this section, we describe the method used for understanding of the heat dissipation from SMA wires and implementation of suitable active cooling mechanisms with focus on robotic systems and unmanned undersea vehicles. We investigated various suitable active cooling techniques such as free and forced convection in air, fluid media and heat sink. Each of these methods were tested and compared with natural convective cooling in ambient air. Figure 2(a) and (b) show the experimental setup used to study the effect of active cooling techniques. The electrical power for driving the SMAs was provided from Agilent Dual output E3648A, DC power supply at the recommended operating values, 180 mA for Flexinol and 200 mA for Biometal. Novotechnik T-Series position sensor with a resolution of 0.002 mm and stroke-length of 50 mm was used to

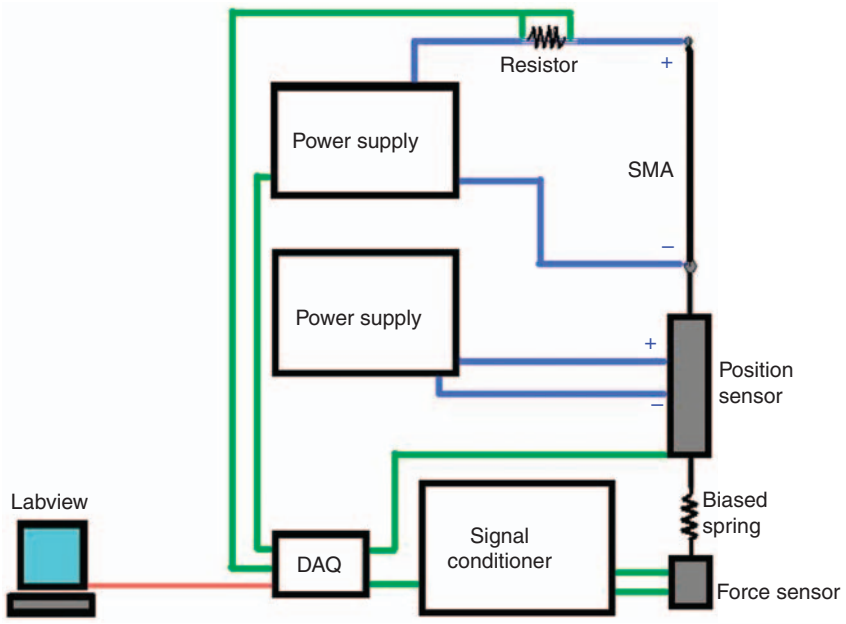

Figure 2. *Schematic diagram of the experimental setup to test active cooling techniques.*

measure the displacement. The SMA wire was mounted to a rigid surface and fixed to the position sensor at one end. The other end of position sensor was connected to force sensor with a bias spring to assist the SMA return to its original position during cooling. Input current was measured by inserting a known resistance in the current loop and measuring the voltage across it. NI 9215 DAQ system with a 4-input voltage module was used to collect the data. A LabVIEW program was created to read the voltages from DAQ at a frequency of 1000 Hz. These voltages were then converted into current, force and displacement using the calibration curves of transducers used in the test. The experiment was conducted on a vibration isolated table to prevent any interference from external sources. All the experiments were under repeated identical conditions to ensure the consistency of measured data.

ACTIVE COOLING EXPERIMENT PROCEDURE

This section describes the procedure for collecting and processing the data on heat dissipation from both Flexinol and Biometal SMA wires. Figure 3(a) shows the setup for characterizing the response time of SMA wire with forced convection. The first low-speed forced air convection at 0.3 m/s was achieved by using a 12 V computer fan and confining the flow within a rectangular channel of dimensions 40 mm width × 89 mm height × 245 mm length. The second high-speed forced air convection was achieved by using a compressor. The experimental setup for high-speed forced air convection is shown in Figure 3(b). The SMA wire was run through an 8.9 mm diameter carbon fiber tube. Air from a compressor was blown through the tube at 4.6 m/s to provide active cooling to the SMA wire. The carbon fiber tube covered almost the entire length of SMA wire, which was in a suspended state inside the tube. Since the velocity of air flow was quite high and the thermal conductivity of carbon is low, we can neglect the heat transfer from SMA wire to the tube. Thus the only heat transfer we need to consider takes place between the SMA wire and the flowing air. The third active cooling method tested was fluid quenching using the experimental setup shown in Figure 3(c). Using the carbon fiber tube, water was injected onto the wire via a syringe at velocity of 2.7 m/s. The heat transfer is proportional to the velocity of quenching. The fourth method implemented was heat sink using the experimental setup shown in Figure 3(d). For this experiment, an aluminum tube was used as a heat sink. As soon as the applied voltage to SMA wire was cut off the tube was allowed to make contact with wire. Careful experimentation was conducted to push the aluminum tube immediately in contact with SMA wire while voltage was being shut down. The aluminum tube was as long as the contracted length of SMA wire (~185 mm) and had a diameter of 26 mm and thickness of 2 mm. The last active cooling method tested was using thermal gel and the test setup is shown in Figure 3(e). This method is similar to that reported by Loh et al. (2000) where the SMA wire was run through a small copper tube that was filled with thermal grease (Arctic Silver) which had a thermal conductivity of 8.9 W/mK. This provides SMA wire large surface area to dissipate heat rapidly. All these experiments shown in Figure 3 were first conducted on Flexinol wire and then the active cooling methods that showed highest decrease in response time

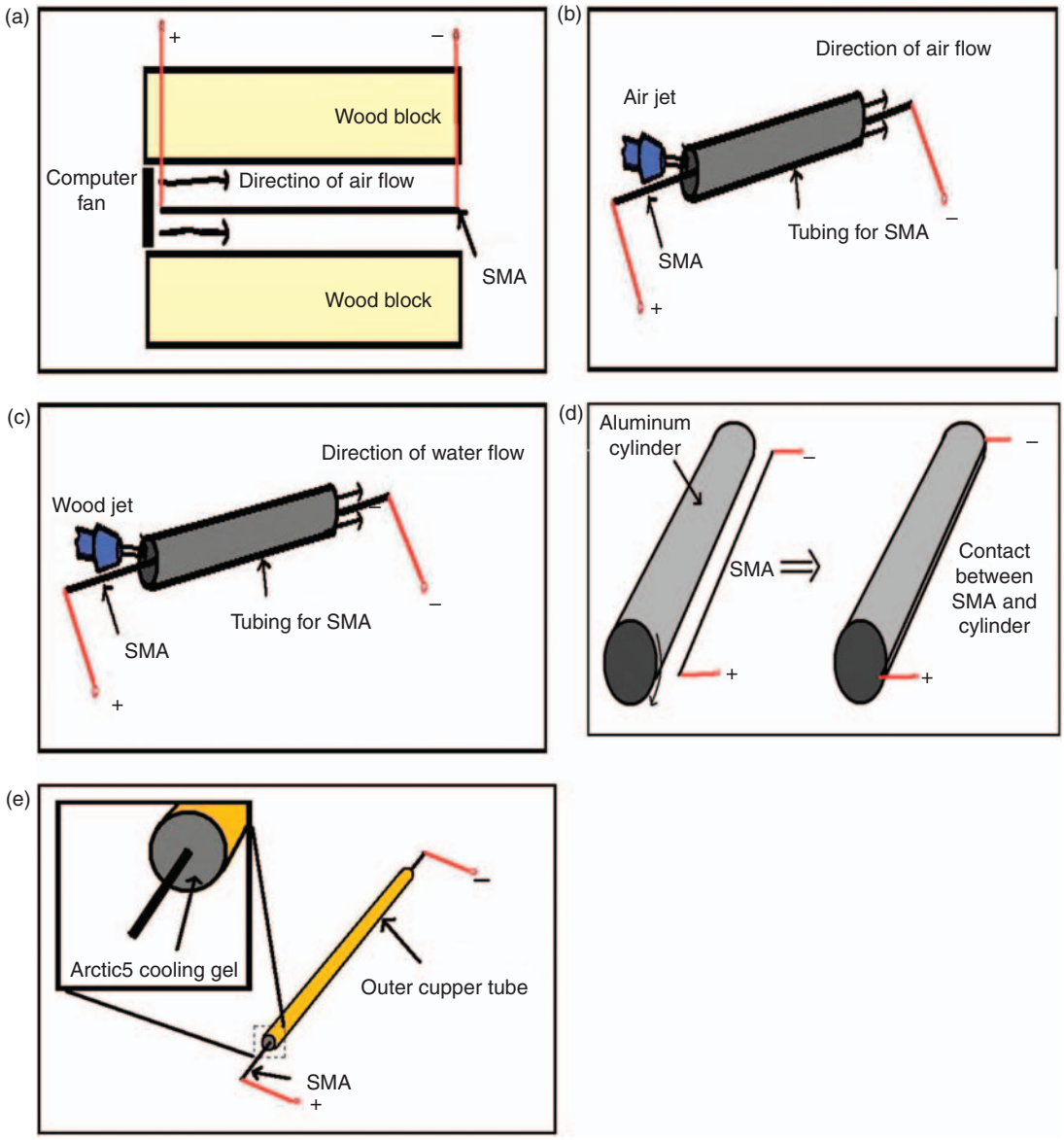

Figure 3. *Illustration of various active cooling: (a) top view of low-speed air active cooling method, (b) high-speed forced air active cooling method, (c) fluid quenching, (d) heat sink cooling method, (e) thermal gel cooling method.*

were experimented on Biometal fiber. After completion of static tests, Flexinol and Biometal fiber were subjected to dynamic current pulses at frequencies of 0.1 or 0.05 Hz to test the effect of multiple actuations on thermal cycle.

Experimental Setup for Pre-stress Characterization

In this section, we describe the experimental setup, measurement procedure and data processing technique used to determine the behavior of two types of SMA actuators, Flexinol and Biometal fiber under pre-stress. The experimental setup consists of Polytec laser vibrometer (Model OFV3001), linear stage, biasing spring, force transducer, and National Instruments data acquisition system (NI 9215) with a computer interface and LabVIEW program. Schematic diagram of experimental setup is shown in Figure 4(a). A SMA wire with ring terminals was attached to biasing spring that was connected to force sensor mounted on a linear stage to detect the force during preloading as well as SMA actuation. Power was supplied to SMA actuator terminal using Agilent Dual output E3648A, power supply. A reflecting tape was attached to the moving point P (as shown in Figure 4(a)). In order to ensure accurate measurement the tape was supported with a vertical plate bent from the terminal of the SMA. The state vector output and input, namely voltage V, force F, and displacement D, were connected to the National instrument data acquisition module interfaced with the LabVIEW program. The time domain response of the displacement and force for various input voltages was

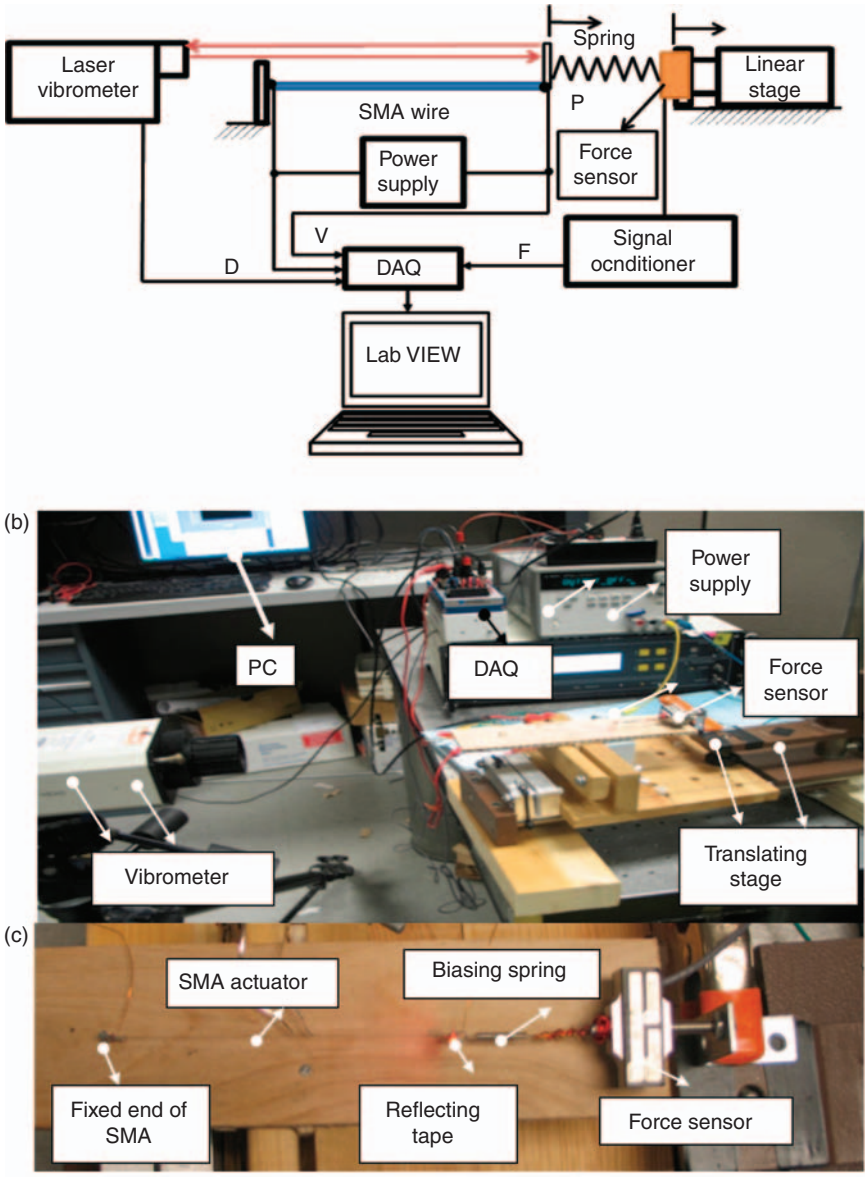

Figure 4. *(a) Schematic diagram of the experimental setup for characterization of the effect of pre-stress; picture of the laboratory experimental setup for pre-stress characterization, (b) isometric view and (c) top view.*

measured using the force transducer and laser vibrometer respectively. Pre-stress was varied by traslating the linear stage in discrete steps and a step DC voltage was applied for 10 s duration across the SMA wire. The experimental data was measured by varying the pre-stress amplitude. The force trasducer was calibrated beforehand and a force conversion factor ($F_s = 972.06\ V_{\text{sen}} + 146.78$) was used to convert the output voltage from trasduction (V_{sen}) to the force (F_s) being measured. The displacement conversion factor for the laser vibrometer used was $d_s = 1.280$ (mm/V). Figure 4(a) and 4(b,c) show the details of experiment and picture of the laboratory setup. It should be noted here that the characterization uses voltage and current stimulus rather than temperature.

RESULTS AND DISCUSSION

Effect of Pre-stress on Response Time

Previously, experimental investigation of deformation-recovery behavior for Ni–Ti–Nb SMA has been reported with emphasis on test temperature dependence (Kusagawa et al., 2001). Monotonic tension and deformation-recovery tests were conducted in temperature range of 253–473 K. It was determined that the dominant mechanism of inelastic deformation was plastic above 323 K and pseudo-elastic below 323 K. It was also shown that strain recovery strongly depends on the magnitude of pre-strain and pre-straining temperature. Larger strain recovery was obtained for larger

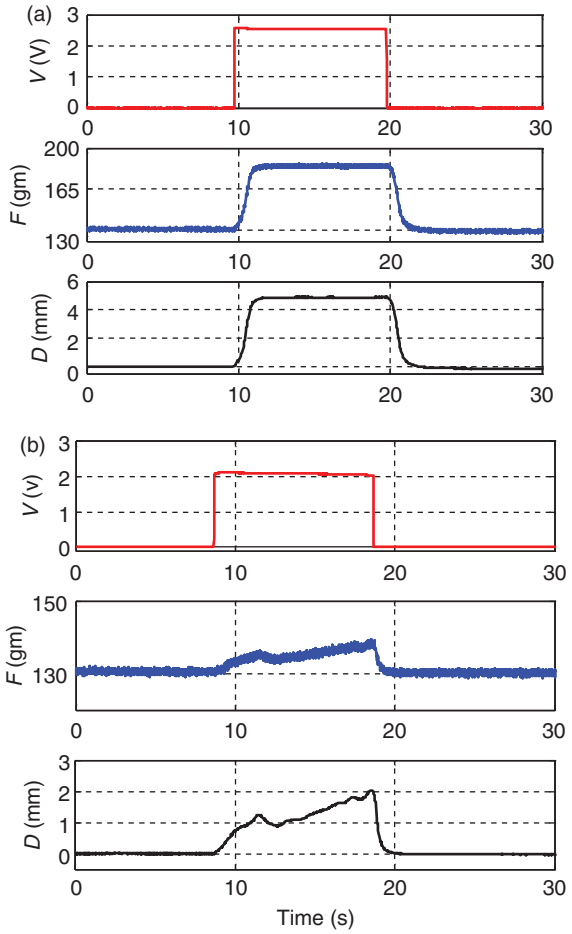

Figure 5. *Typical state vector (force, displacement, voltage, time) showing force and displacement at certain step input voltage and 130 gf pre-stress condition: (a) 100 μm diameter Biometal fiber and (b) 100 μm diameter Flexinol wire.*

pre-strain at lower pre-straining temperatures. Wada and Liu (2005) have investigated thermally induced shape recovery behavior of Ni–Ti SMAs under both constant pre-strain with variable constrained stress and constant constrained stress with variable pre-strain. It was shown that the development of maximum strain is independent of deformation procedures and is mainly determined by the magnitude of martensitic strain generated during either pre-deformation or thermal cycling.

A study conducted on phase transformation behavior of pre-strained Ni–Ti SMA in reinforced metal matrix indicated that the recovery stress is dependent upon the heating cycle. A higher recovery stress was obtained in the first heating cycle than the subsequent ones. The mechanism for this phenomenon was identified in terms of changes in the microstructure in relation to the parent phase (Li et al., 2001). Pre-straining increases the transformation temperatures of Ni–Ti SMAs and both theoretical and experimental studies have shown the shift in transformation temperature. A large increase in the transformation temperature during the heating cycle with just 0.5% pre-strain has been reported in Ni–Ti SMA (Huang and Wong, 1999).

Figure 5(a) and (b) show the typical variation of state variables, output displacement and force for specific input voltage. The data is shown for both Flexinol and Biometal fiber actuators for a tyical magnitude of pre-load force of 130 g. It can be observed in this figure that the response time of force and diplacement of Flexinol is slower than the Biometal fiber. Generally at zero pre-stress, SMA actuators produce highest force with the fastest rise time which decreases as the pre-stress is increased. This can be quantified by the change in slope of output force and displacement. Figure 6(a) shows the force and corresponding displacement of Biometal fiber under varying pre-loading force. It can be noticed from this figure that for wide range of pre-loading force: (i) amplitude of generated force was nearly constant, (ii) slope change was small, and (iii) displacement range was 4–4.7 mm (4% strain). Figure 6(b) and (c) shows the variation of displacement and force output for the Flexinol actuator with two different diameters of 100 μm (0.004 in.) and 127 μm (0.005 in.). The results in these figures show that: (i) amplitude of output force decreases as the pre-loading increases, (ii) slope of force generation with respect to time axis was much higher than that of Biometal fiber, and (iii) displacement amplitude decreases as the preloading was increased with higher slope compared to Biometal fiber. The results of Figure 6 show that under identical driving and pre-loading conditions, Biometal fiber provides better response time with smaller degradation in magnitude of displacement and force. It is to be noted that the initial elongation of the actuator due to pre-stress was deducted and the displacement due to actuation is presented in each displacement diagram.

Magnified views of both rising and falling edge of displacement response for Biometal fiber is shown in Figure 7(a), indicating that the rise time is in range of 0.8–2 s and fall time between 1 and 1.6 s for pre-stress in the range of 0–245 gf. The *rise time* is defined here as the time required for attaining a steady state output and the *fall time* is the time required to cool and reach original position before application of step input voltage. Figure 7(b) and (c) demonstrate the rise and fall time of displacement for the Flexinol actuator with two different diameters of 100 and 127 μm. The results for 127 μm diameter indicate that the displacement slope increases significantly as pre-stress increases. The rise time in this case is in range of 4–6 s and fall time between 1.5 and 2 s for pre-stress between 0 and 220 gf. In the case of 100 μm diameter, the rise time ranges between 3 and 10 s and the fall time between 1 and 1.5 s depending upon the pre-stress.

If the rising edge takes T_r second and falling edge takes T_f second, then the maximum working frequency

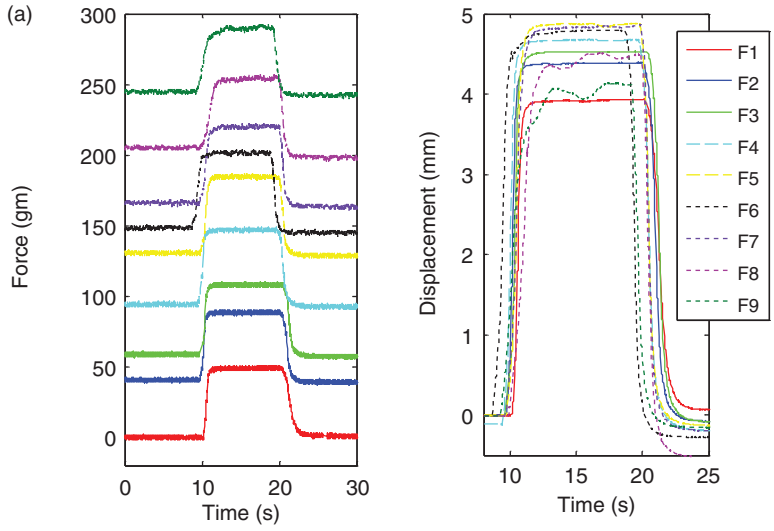

F1=0; F2=41; F3=59; F4=94; F5=131; F6=148.5; F7=166.5; F8=205; F9=245 gf

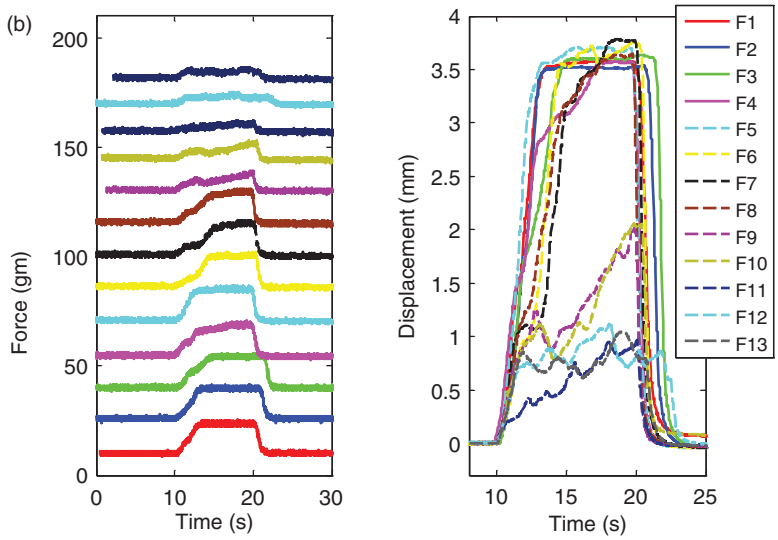

F1=10; F2=26; F3=40; F4=55; F5=71; F6=87; F7=101; F8=116; F9=131; F10=145; F11=158; F12=170; F13=182 gf

Figure 6. *Force and displacement characteristics of (a) 100 μm diameter Biometal fiber, (b) 100 μm diameter Flexinol, and (c) 127 μm diameter Flexinol actuator.*

of SMA actuator can be computed from: $f_{\max} = 1/(T_r + T_f)$. The frequency of operation without losing the force generation capability would be 0.28–0.55 Hz for Biometal fiber, 0.13–0.18 Hz for 127 μm Flexinol wire, and 0.08–0.25 Hz for 100 μm Flexinol wire depending upon the preloading stress. Further analysis of the force response of SMA wire leads to the force generation rate as a function of pre-stress load. It was demonstrated in Figures 6 and 7 that the output force for Flexinol decreases appreciably with pre-stress while that for Biometal remains nearly constant. The relationship between pre-stress amplitude and force generation rate is illustrated in Figure 8. Flexinol force generation rate was of the order of 1–7 MPa/s for a pre-stress range of 0–160 MPa whereas for Biometal fiber the force generation rate was 10–80 MPa/sec in preload range of 0–320 MPa. Figure 8 also shows the resulting nonlinear relationship between response time and preload condition.

The response time of both Flexinol and Biometal fiber becomes faster as the voltage is increased under a specific pre-stress. To illustrate this phenomenon, for a Biometal fiber actuator under a pre-load of 60 gm, the recommended driving voltage results increase in voltage level did not provide any significant improvement in rise time except slight increase in the amplitude in both displacement and force. Figure 9(a) (i–iii) demonstrates the relationship between response time achieved by voltage

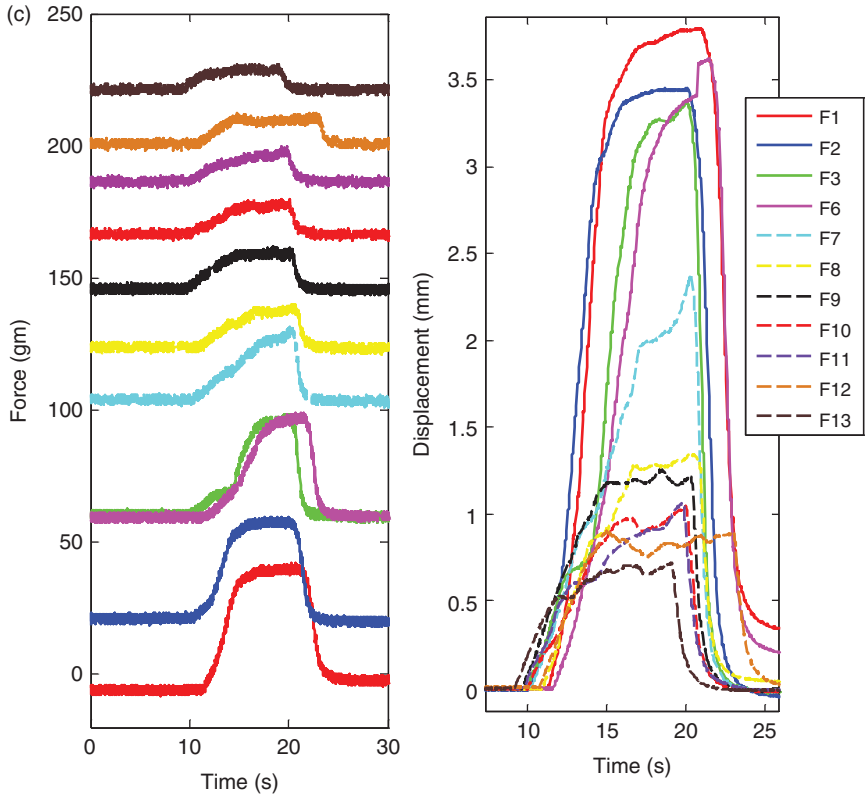

F1=0; F2=21; F3=59.5; F6=60.5; F7=104; F8=124; F9=146; F10=167; F11=187; F12=201; F13=221.5 gf

Figure 6. *Continued.*

compensation in terms of stress–strain diagram through three dimensional relationships of stress, strain, and time for applied voltage levels of 2.86, 3.79, and 4.72V. Similar measurements were conducted for Flexinol actuator as shown in Figure 9(b) (i–iii); however, in this case the recommended voltage resulted in delay, which could be compensated by increasing the driving voltage level.

Comparing the results from Figures 6–9, it can be seen that Flexinol exhibits higher rise time with pre-stress and takes longer duration to reach steady state. On the other hand Biometal fiber shows almost constant rise time with pre-stress. At the applied pre-stress of greater than 175 gf, the force–time response is significantly reduced for Flexinol while Biometal fiber can exhibit constant magnitude of force generation until 250 gf. The displacement for both Biometal fiber and Flexinol increases with stress and then decreases. However, in case of Flexinol the displacement decreases by more than 57% as compared to 20% for Biometal fiber with increase in 200 gf pre-stress (total length of SMA = 100 mm). Further, at these higher pre-stress magnitudes, Biometal fiber reaches steady state faster than Flexinol. It was found that under load of 50 gf, Flexinol requires additional driving voltage to reach the steady state response. All the force generation and displacement results can be explained in terms of Equation (5), which shows that the fraction transformation from martensite to austenite (and vice versa) is dependent upon the transformation temperatures, slope of the stress–temperature diagram, and superelastic behavior. It is evident that the material compositions and processing conditions of these commercial alloys is different leading to changes in the magnitude of a_A, C_A, a_M, and C_M. Since Equation (5b) is nonlinear, a small difference in the magnitude of these parameters can lead to large difference in the rate of fraction of austenite. Further, the magnitude is typically influenced by the difference between the rate of change of temperature and stress states along with the associated material constants. The magnitude of cosine function will remain between 0 and 1. As the pre-stress increases, the difference between the rate of change of temperature and stress becomes close to zero leading to no phase transformation. These results show that Biometal fiber can provide consistent force–displacement relationship in applications where there is presence of non-zero pre-stress. Other behaviors such as cyclic actuation and fatigue under various pre-stress conditions of Biometal fiber and Flexinol need to be further investigated. Certain representative cyclic behavior will be discussed in the section 'Cyclic Actuation.'

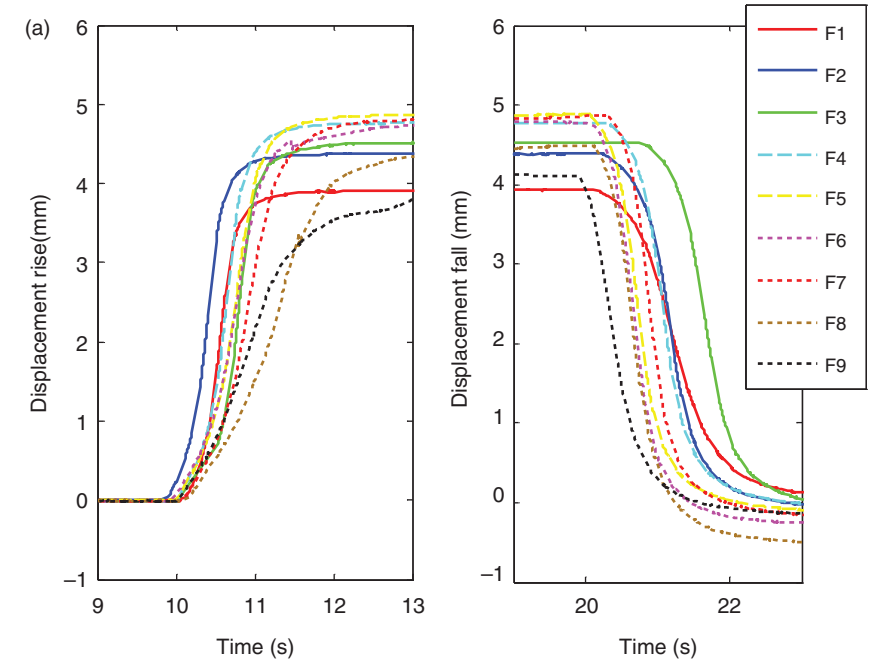

F1=0; F2=41; F3=59; F4=94; F5=131; F6=148.5; F7=166.5; F8=205; F9=245gf

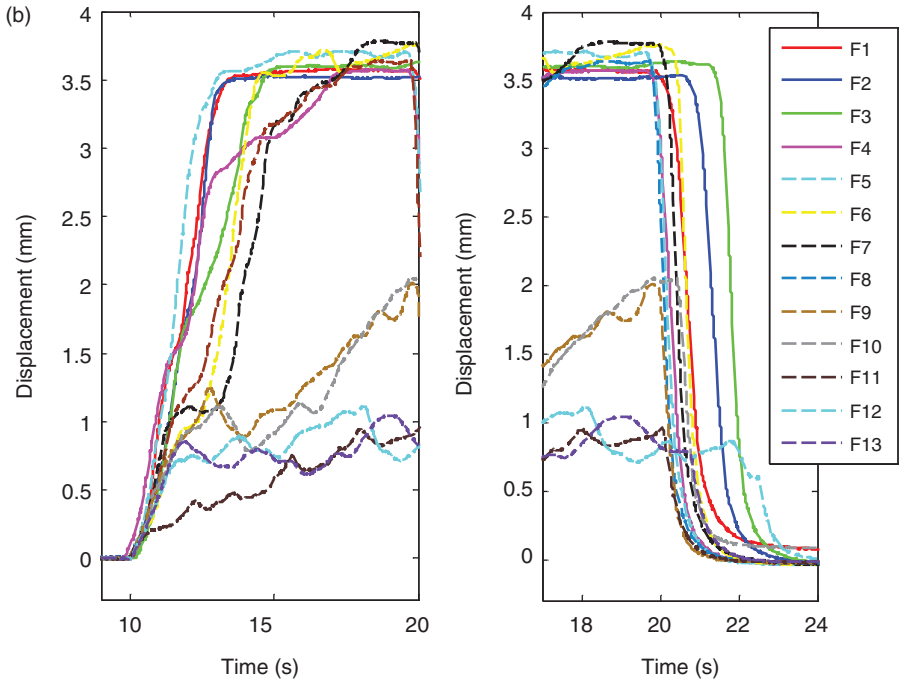

F1=10; F2=26; F3=40; F4=55; F5=71; F6=87; F7=101; F8=116; F9=131; F10=145; F11=158; F12=170; F13=182 gf

Figure 7. *Magnified view of the rise and fall time of (a) 100 μm diameter Biometal fiber, (b) 100 μm diameter Flexinol actuator, (c) 127 μm diameter Flexinol wire for step input voltage under varying pre-stress.*

Effect of Active Cooling Techniques on Response Time

In this section, the response time of SMAs is compared utilizing the active cooling methods described earlier as well as variable initial conditions. Figure 10 shows the comparison between various methods of active cooling and the changes in profile of thermal response of a 195 mm long, (i) 127 μm diameter and (ii) 100 μm diameter Flexinol wire while being cooled from maximum strain state. The black line shows the response of SMA wire with no active cooling (ambient cooling) and as is evident from the figure that it takes the longest time

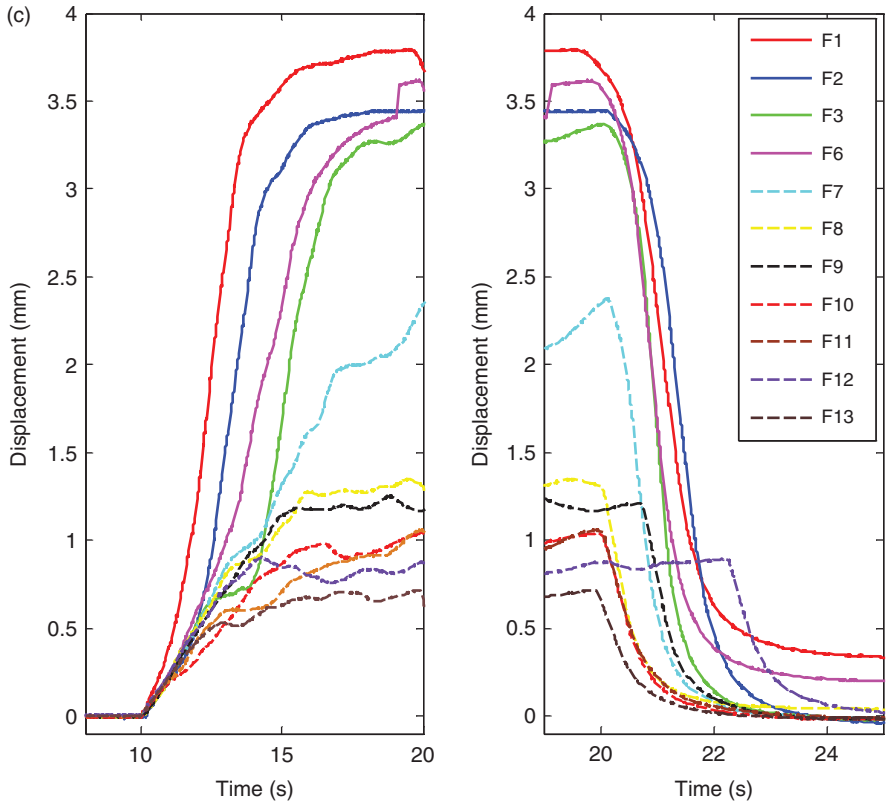

F1=0; F2=21; F3=59.5; F6=60.5; F7=104; F8=124; F9=146; F10=167; F11=187; F12=201; F13= 221.5 gf

Figure 7. *Continued.*

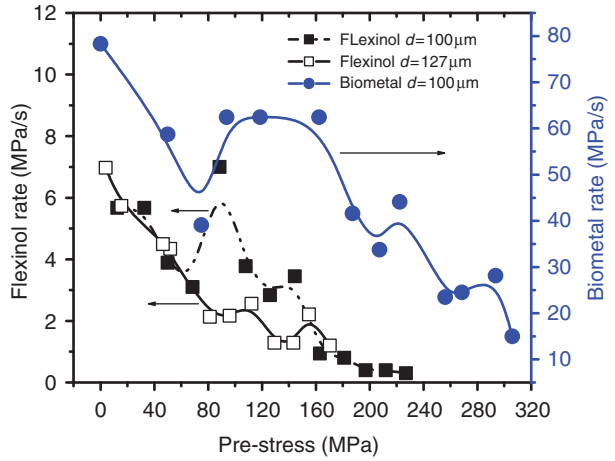

Figure 8. *Force generation rate for pre-stress applied on SMA actuators. Note that the left axis is for Flexinol actuator and the right axis is for the Biometal fiber.*

to reach the undeformed state (~1.6 s to reach zero percent strain). The low-speed forced air cooling had a small effect on the response time, reducing it by 0.5 s as compared to ambient cooling. This may be due to the fact that the fan needs some time itself to achieve maximum velocity. It may also be related to the fact that air flow takes some time to reach the end of channel where SMA is mounted.

The data for thermal gel was neglected because the SMA wire failed to contract. This can be explained as following: (i) the thermal gel is dissipating heat rapidly during contraction and thus the wire cannot retain enough heat to contract completely, and (ii) the SMA could not produce enough force to overcome the viscosity of thermal gel. Contraction was eventually produced by increasing the magnitude of current running through the wire to 2 A. However, this is practically not useful and thus the active cooling using thermal gel will not be discussed further in this manuscript. The other three methods of active cooling, namely, high-speed forced air, heat sink, and high-speed fluid quenching were found to be the most effective ones. High- speed fluid quenching reduces the cooling time from 1.6 to 0.2 s while the heat sink and forced air reduced the cooling time to 0.4 s. The smaller wire leads to faster cooling times due to less energy being contained within the wire. It is expected that Biometal fiber will follow a similar trend as a function of diameter.

Figure 11(a)–(c) compares the thermal response times for Flexinol and Biometal fiber using active cooling based on forced air, heat sink, and fluid quenching.

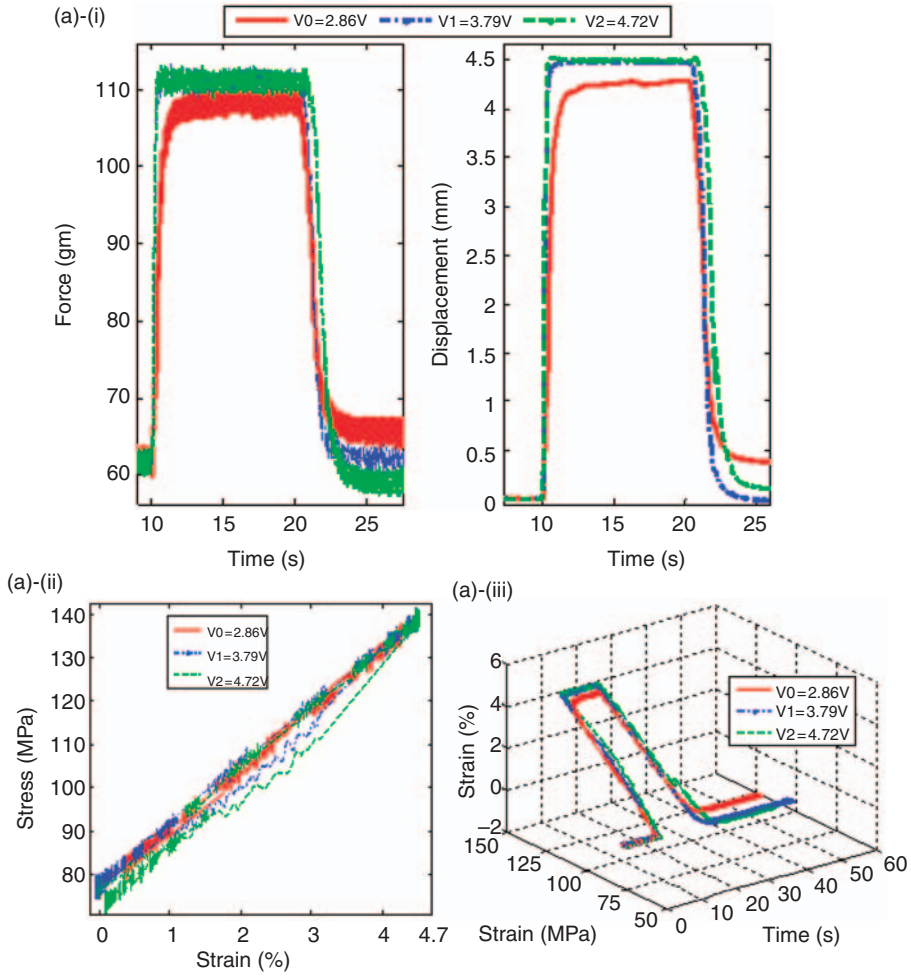

Figure 9. *Response characteristics under 50 g preload force and variable amplitude of input voltage: (a) Biometal fiber actuator and (b) Flexinol. The italic number for each case represents (i) time domain force and displacement for step input, (ii) stress–strain diagram, and (iii) the three dimensional relationship between strain, stress, and time.*

The Biometal fiber did not reach the same level of displacement as Flexinol. This may be related to slight difference in pretension of the wire and can be determined using the results presented in Figure 6. Since the transformation temperature of Biometal wire (70°C) is 20°C less than that of Flexinol (as can be seen in Table 2), it shows faster response time in all of these three active cooling methods. These results are quite interesting and in conjunction with the results presented in previous section, it can be summarized that response time of Biometal fiber can be increased (reducing the delay) by active cooling and over a wide range of pre-stress condition without significantly affecting the generated force–displacement.

ENERGY DISSIPATION DURING HEATING

SMA wires contract due to phase change from martensite to austenite, which is dependent upon the temperature. Therefore, if a wire is dissipating heat while it is being heated, the phase change will not occur unless the heating method is generating enough energy to overcome the dissipation. Since SMAs are traditionally heated by passing current through the wire, the effects of heat dissipation can be overcome by passing more current through the wire. Figure 12 demonstrates the enhancement of strain by increasing the current with continuous dissipation. This figure shows the strain in Flexinol wire at different currents under low-speed forced air convection. In this case, an increase in current by 44 mA results in increase of the strain from 1% to 3.3%, while the computer fan was on during the heating cycle. Since our goal is to find the best method for increasing the response time while keeping the electrical power consumption small, we can conclude that any cooling during the heating cycle will negatively affect the system performance.

MARTENSITE FRACTION

The fraction of martensite can be determined indirectly from temperature versus time behavior during

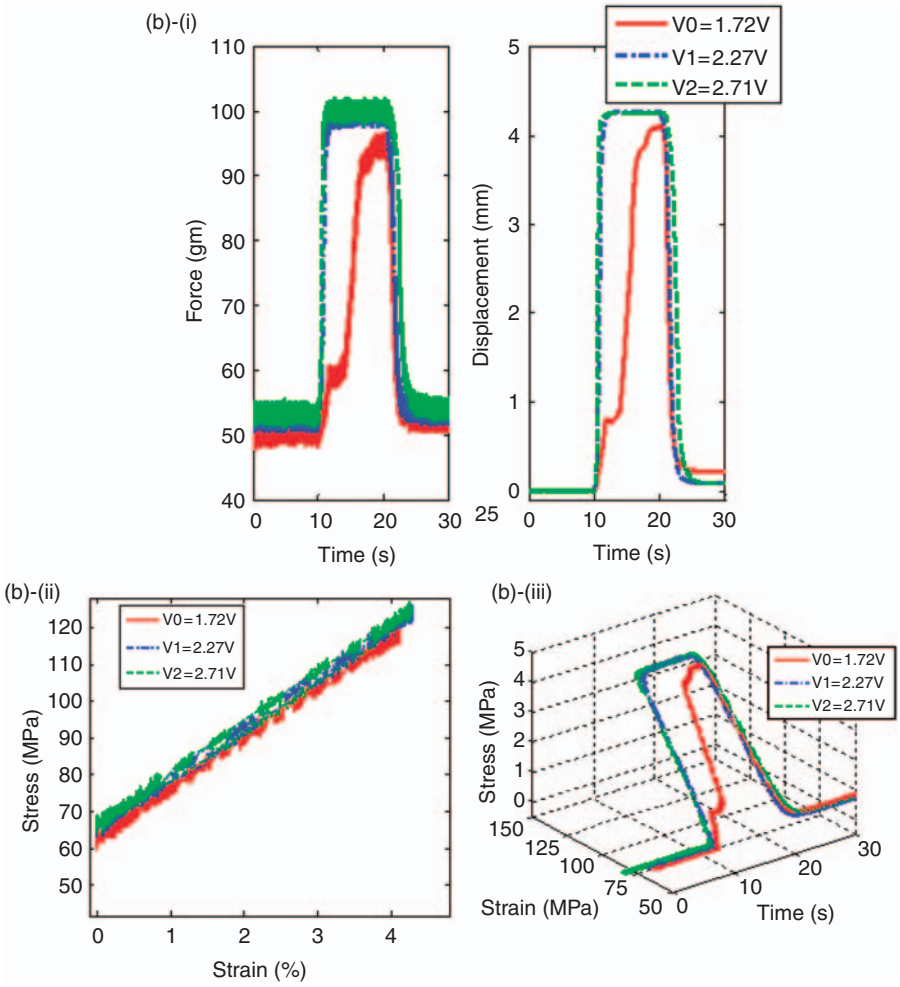

Figure 9. *Continued.*

heating and cooling in combination with Equation (3). The required temperature versus time curve can be obtained by creating a relationship between two sets of experimental data corresponding to strain versus time and strain vs. temperature.

The strain versus temperature behavior of SMA during heating and cooling cycle is shown in Figure 13. In this case, the strain data was recorded by a position sensor while the SMA was being heated in a furnace. The furnace was heated from room temperature (26°C) to 150°C and then cooled again to room temperature. A standard K-Type thermocouple was used for measuring the temperature. The temperature and strain data were collected multiple times using the same DAQ system as in the previous experiment to confirm the behavior. The graphs shown in Figure 13(a) and (b) are average results from multiple repetitions for both Flexinol and Biometal fiber, respectively. By fitting a polynomial curve to the cooling cycles, a relationship between strain and temperature can be obtained for both types of SMAs. Equations (8a) and (9b) are given for Biometal fiber and Flexinol, respectively. This equation can then be used to transform the strain versus time data, which was measured for various active cooling methods separately into temperature versus time data.

$$T = 0.078\varepsilon^5 - 0.86\varepsilon^4 + 4.7\varepsilon^3 - 15\varepsilon^2 + 28\varepsilon + 36, \quad (9a)$$

$$T = -0.057\varepsilon^4 + 0.68\varepsilon^3 - 1.6\varepsilon^2 + 2\varepsilon + 50. \quad (9b)$$

Once the temperature profile as a function of time, $T(t)$, is known it can be inserted into Equation (3). The characteristic temperatures, M_s and M_f can be found from Figure 13 (Biometal: $M_s = 85°C$, $M_f = 45°C$ and Flexinol: $M_s = 68°C$, $M_f = 49°C$) while a commonly used average value of $C_M = 8\,\text{MPa}/°C$ for Flexinol (Nascimento and Araujo 2006; Zhou and Yoon, 2006) and $C_M = 5.88\,\text{MPa}/°C$ was taken from the slope of stress versus transformation temperature for Biometal fiber. The stress was calculated from the

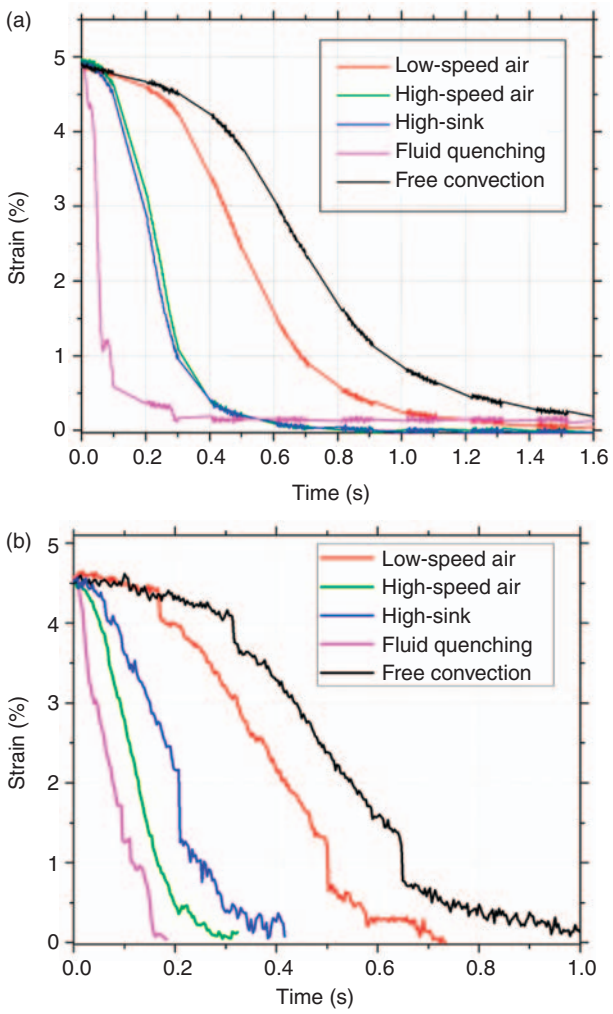

Figure 10. *The thermal response times of Flexinol SMA wire for four active cooling methods: (a) 127 μm diameter, and (b) 100 μm diameter.*

deformation length of biasing spring (172 MPa). Figure 14(a) and (b) shows the variation of martensite fraction as a function of time calculate using Equation (3b)

As can be observed from Figure 14(a-i) and (a-ii) that both Biometal and Flexinol exhibited fastest transformation from austenite to martensite during fluid quenching. Using the data in this figure, strain versus. martensite fraction plot can be constructed as shown in Figure 14(b) for both Flexinol and Biometal fiber. Figure 14(b) is characteristic curve for various methods of cooling investigated in this study because the martensite fraction is directly related to the percent strain generated. It can also be observed from this figure that Biometal fiber exhibits zero martensite fraction at lower strain magnitude which implies that Flexinol has slightly higher contraction.

HEAT TRANSFER ANALYSIS

It is interesting to compute the heat dissipation from SMA wire as a function of time. In order to use the lumped capacitance parameter model given by Equation (6), it is important to satisfy the criterion used in its derivation. For a given characteristic length, $L_C = 2.54 \times 10^{-5}$ (given by wire volume over surface area) and thermal conductivity of the wire, $K = 18$, the Biot number (Bi) must be less than 0.1. Substituting these parameters in Equation (6), the inequality for heat transfer coefficient can be obtained as $h < 70867\,\mathrm{W/m^2K}$. Since this h value is much higher than that can be achieved in the experiment, the lumped capacitance model can be assumed to be valid. Using Equation (8), the heat transfer constant (h_o) was obtained by fitting the experimental data for temperature as a function of time for each active cooling method and the values are listed in Table 3. In this calculation the magnitude of density was taken to be $6450\,\mathrm{kg/m^3}$, heat capacity was taken to be $322\,\mathrm{J/kg\ K}$, and the ambient temperature was taken as the martensite finish transformation temperature of 50°C. To put it in perspective, a human hand has an average heat transfer coefficient of $6\,\mathrm{W/m^2K}$ and a steam turbine has an average heat transfer coefficient of $1200\,\mathrm{W/m^2K}$. In literature (Luo et al., 2000; Nascimento et al., 2006, Leo, 2007), heat transfer coefficient for thermomechanical response of SMA is considered to be constant. For variable heat transfer coefficient which depends on environmental conditions and temperature of wire, a second order polynomial function can be used (Jayender et al., 2005; Moallem and Tabrizi, 2009) as given by Equation (10):

$$h = h_0 + \beta T^2, \tag{10}$$

where h_0 is the constant value for heat transfer coefficient, β is the temperature coefficient and T is the temperature of the SMA wire. The magnitude of h shows a significant variation in the range of $185–2800\,\mathrm{W/m^2K}$ as shown in Table 3. Figure 15 shows the measured temperature–time response and the fitted temperature profile by using different magnitudes of constant and variable heat transfer coefficients. As shown in each case, using a constant h value in Equation (8) provides a temperature profile with reasonable accuracy. Variable heat transfer coefficients leads to a better estimate of the temperature profile mimicking the realistic condition. The coefficients of the heat transfer were also obtained by solving Equations (7) and (10) in Simulink and Matlab and are compared with experimental values. It can be inferred from Figure 15 that the values of temperature coefficient are negative and small in magnitude. We can also see that variable heat transfer coefficient closely matches with experimental data.

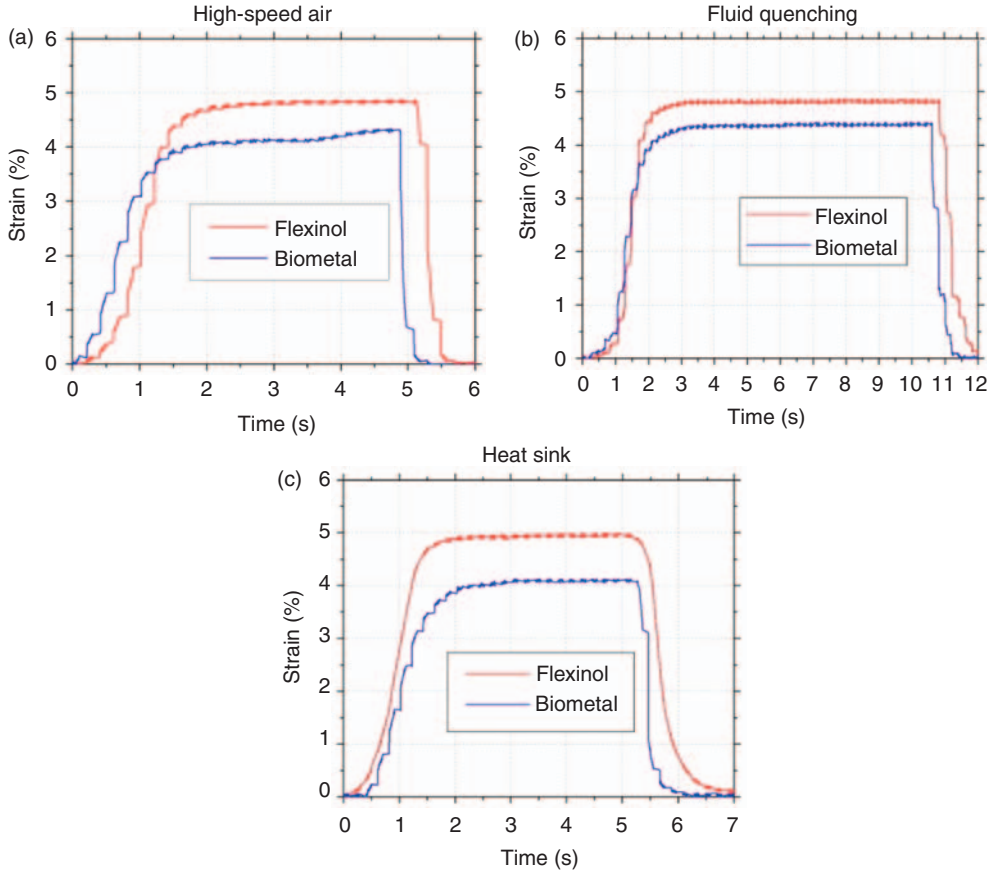

Figure 11. *Comparison of response times for Flexinol and Biometal wires with three different active cooling methods: (a) high-speed forced air, (b) fluid quenching, and (c) heat sink.*

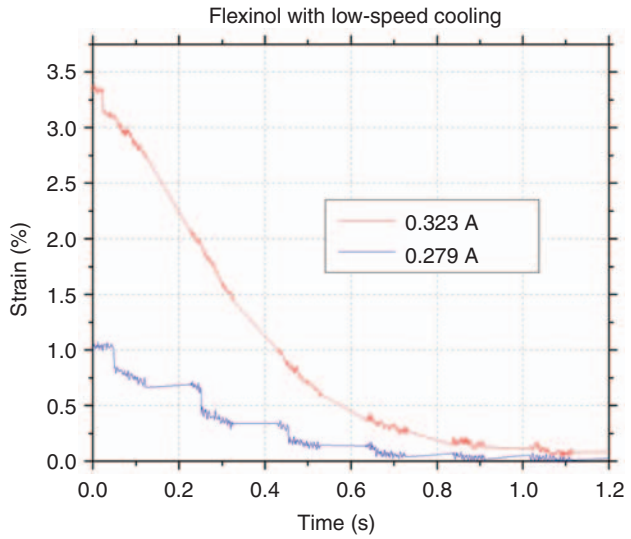

Figure 12. *Behavior of SMA wires for low-speed air cooling methods during the heating phase with two current amplitude.*

CYCLIC ACTUATION

The cyclic actuation behavior of SMA wires for various active cooling methods was investigated because many systems require operation over extended period of time. The SMA wires were subjected to square wave of 0.1 Hz for forced air and heat sink testing and a square wave of 0.05 Hz for fluid quenching test. The extra time between the contractions for fluid quenching test was necessary to remove excess water from the tube before the next contraction cycle. The results from these tests are shown in Figure 16(a–c). This figure shows that the Flexinol wire maintains its strain characteristics over repeated actuation cycles while the Biometal fiber shows a shift in performance especially in the forced air active cooling method. As the SMA wire is repeatedly contracted, some energy from the previous actuation is stored in the SMA wire, which causes shifts in the strain. There is a slight decrease in the magnitude of contraction but most of the effect was exhibited in the shifting of contraction. This result indicates that Flexinol wire would be better in repeated cycle application.

The cyclic actuation lifetime of SMA under pre-stress is highly dependent on the magnitude of applied stress (Kumar et al., 2006). This limit is imposed by permanent plastic deformation resulting from fatigue. The fatigue behavior of SMA is dependent upon the stress amplitude, frequency of actuation, operating environment and mounting conditions (Tobushi et al., 2000). Experimental investigation on the fatigue behavior of

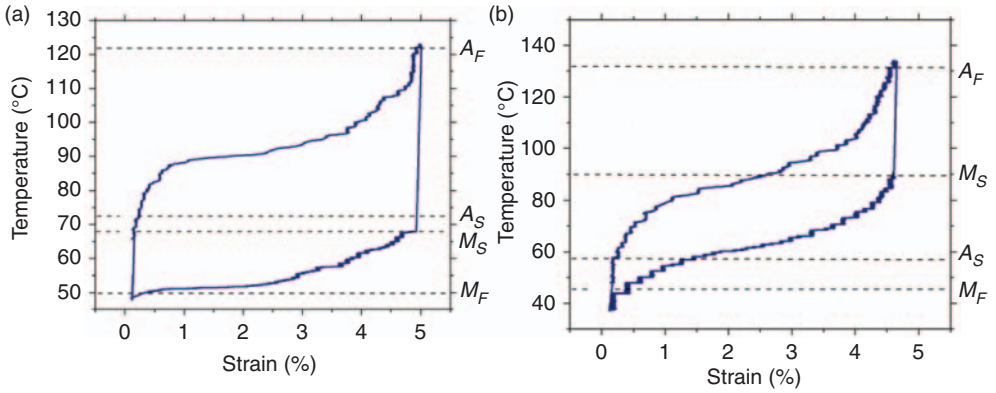

Figure 13. *Experimental heating and cooling curves for (a) Flexinol and (b) Biometal.*

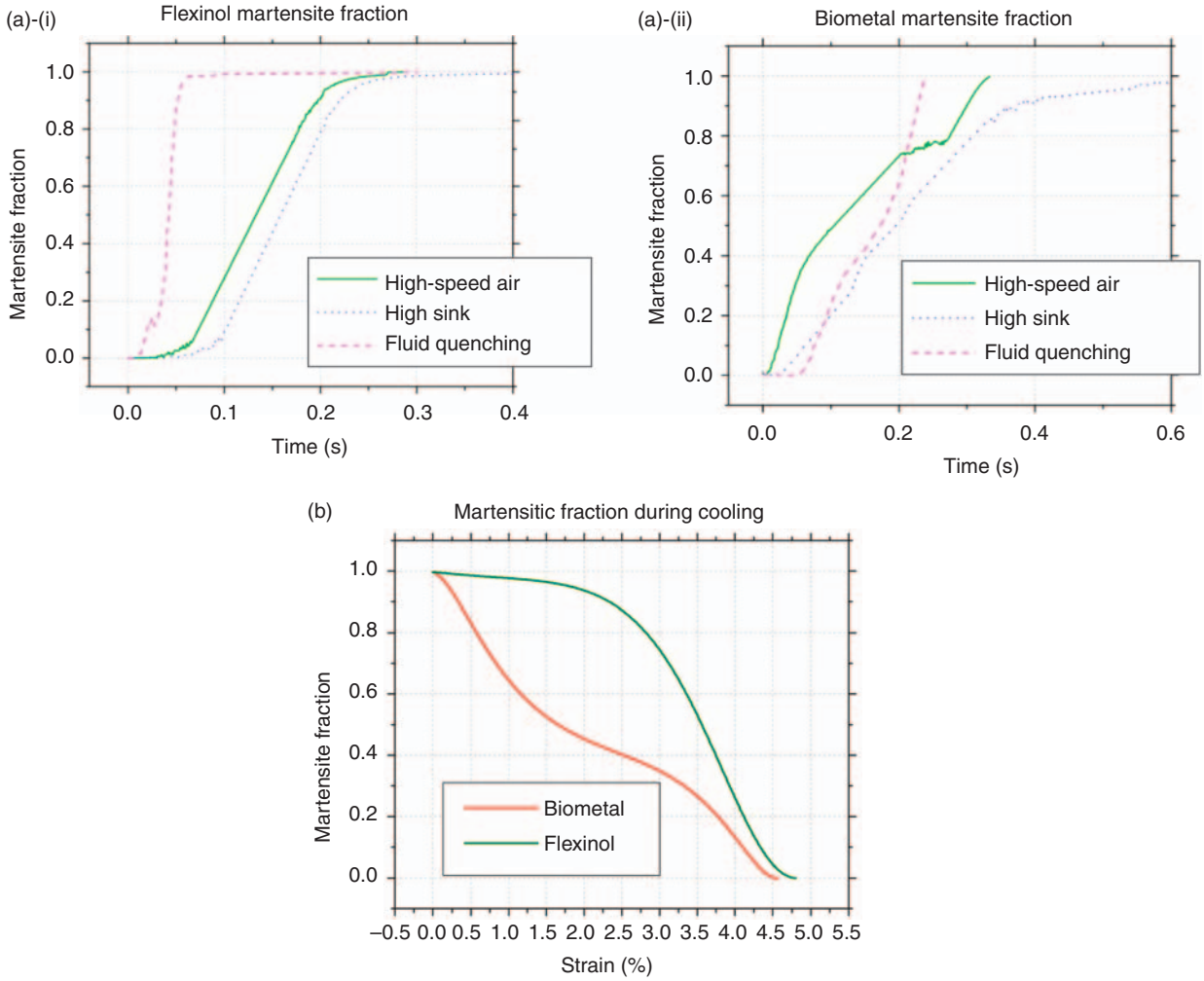

Figure 14. *(a) Fraction of martensite vs transition time behavior for (i) Flexinol and (ii) Biometal fiber, (b) martensite fraction vs. strain curves for 0.005″ diameter Flexinol and Biometal fiber.*

SMA actuator based on NiTiCu wires have been conducted in the applied stress range of 50–250 MPa by Lagoudas et al. (2009). It was found that the fatigue life decreases as the stress amplitude increases. The number of cycles to fail at a high stress level of 200 MPa was on the order of ~2000 cycles which increases to ~30,000 cycles by reducing the stress level to 25 MPa. Bertacchini et al. (2008) have conducted fatigue testing on 'nickel-rich' NiTi SMA actuator in a stress range of 100–250 MPa showing fatigue limit of

Table 3. Heat transfer coefficients for various active cooling methods for Flexinol wire.

Cooling method	Constant heat transfer coefficient $h = h_0$ (W/m^{2}K)	Variable heat transfer coefficient ($h = h_0 + \beta T^2$)
Fluid quenching	2800	−0.3
High speed conv.	800	−0.1
Heat sink	650	−0.09
Low speed conv.	300	−0.04
Free	185	−0.02

5000 to 60,000 cycles. Thus, higher nickel concentration improves the fatigue limit of SMA. Fatigue testing on $Ni_{50.1}Ti_{49.9}$ and $Ni_{50.7}Ti_{49.7}$ demonstrated that the number of cycles to failure were in the range of 10^3 and 10^4 when strain was in between 4% and 5% (McNichols and Brooks, 1981). From these results, it can be concluded that for an applied stress higher than 200 MPa or strain more than 4%, the number of useful cycles are in the vicinity of ~1000.

FUTURE WORK/IMPLEMENTATION

The implementation of active cooling method and pre-stressing of SMA wire in applications such as

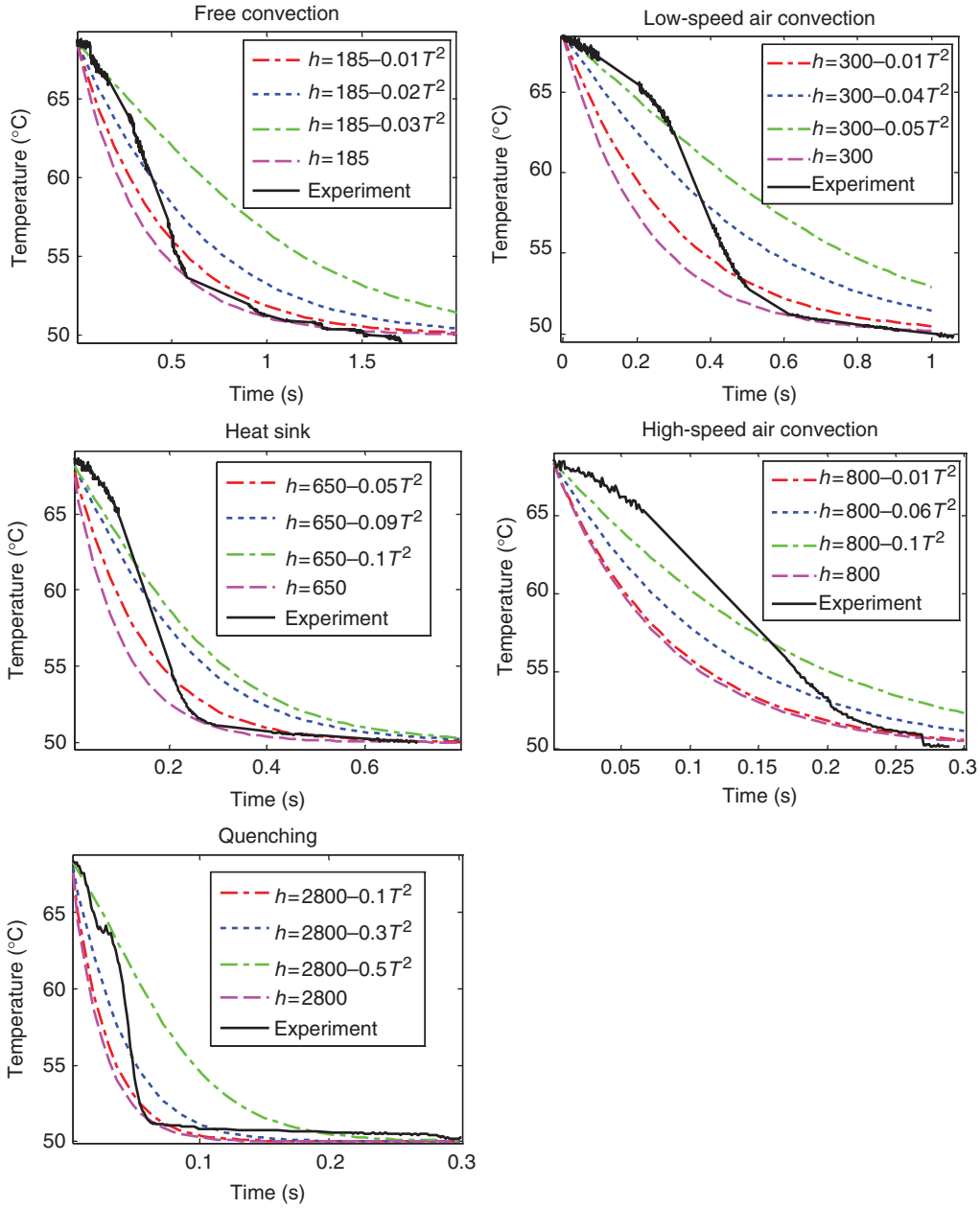

Figure 15. *Constant and variable convective heat transfer coefficients for various active cooling techniques.*

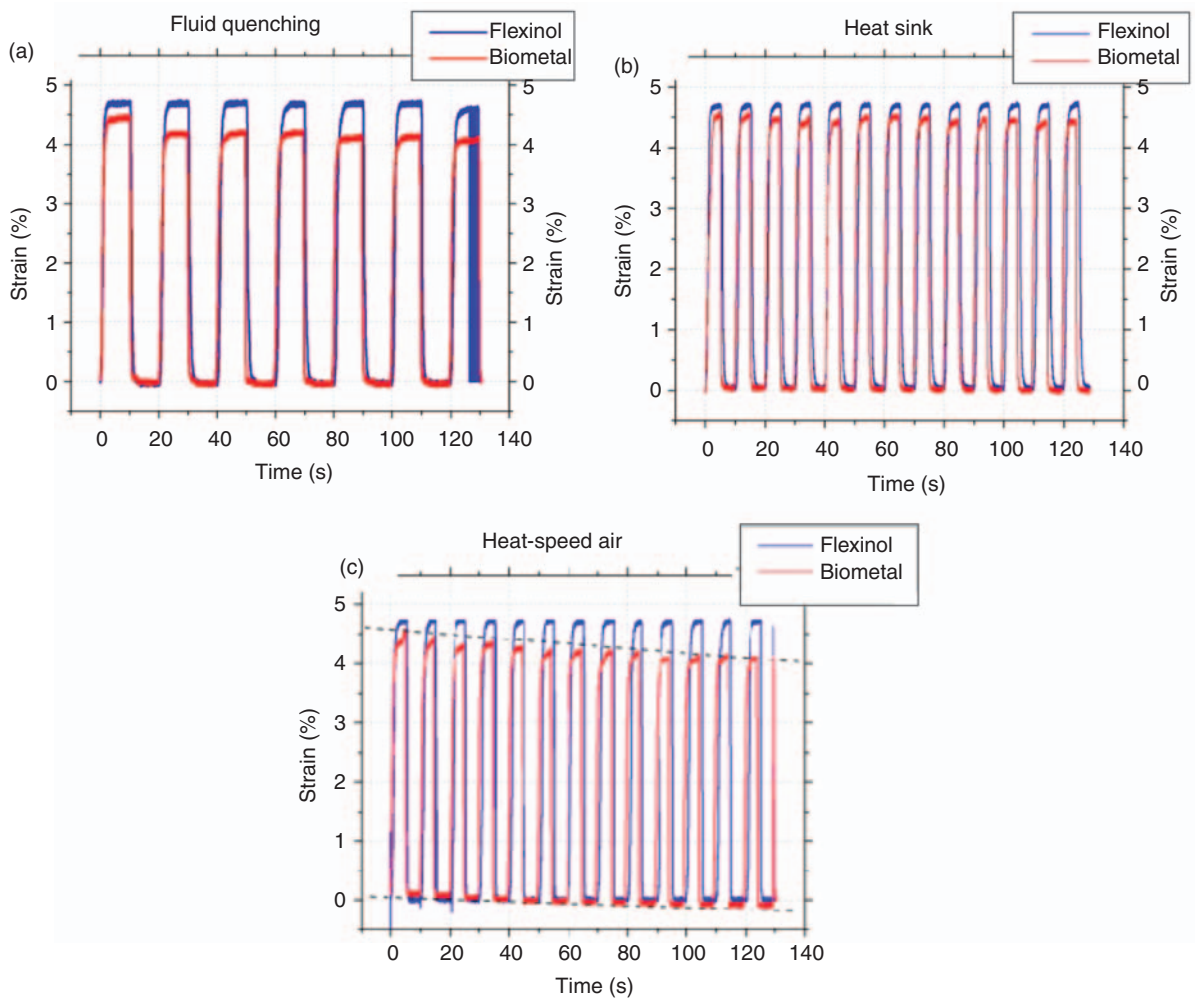

Figure 16. *Thermal response of Biometal fiber and Flexinol under multiple heating/cooling cycles with (a) fluid quenching, (b) heat sinking, and (c) high-speed forced air cooling.*

robotics systems and unmanned undersea vehicle, to enhance its performance needs to be investigated. As shown in Figure 17, the cooling mechanism can be implemented in humanoid face that is capable of displaying emotions through pulling of SMA wire-based artificial muscles. The human face is capable of producing motions at frequencies of 6–7 Hz. Therefore, the enhancement of response time of SMA wires makes this actuator suitable in this application. The mechanism shown in Figure 17 utilizes the SP 135 FZ micro vane pump to induce flow through a channel where SMA wire resides. The SP 135 FZ micro vane pump has dimensions of 27 mm length and 15 mm in diameter. As the SMA wire contracts it will depress the bias spring located within the channel. Since the current is no longer applied to the wire, the SP 135 FZ will create a vacuum and allow air to flow in the channel thus resulting in cooling of the wire. The spring is placed to help the wire return to its normal equilibrium position as well as to maintain the tension in wire at all times.

CONCLUSIONS

Pre-stress dependence of force and displacement was investigated for two commonly utilized SMA actuators, Flexinol and Biometal. The time domain response of actuators was measured by applying recommended step input voltage. The results show that Biometal fiber can be used for relatively higher operating frequencies. Without compromising the force generation capability, highest frequency of operation was found to be 0.55 Hz for 100 μm diameter Biometal fibers (BMF100), 0.25 Hz for 127 μm diameter Flexinol, and 0.18 Hz for 100 μm diameter Flexinol. Compared to Biometal fiber, the strain rate (slope of displacement curve with respect to time) decreases faster for Flexinol as the preloading increases. Further, Biometal fiber was found to generate nearly constant amplitude of force and displacement under varying range of pre-stress whereas Flexinol actuator shows decrement as the pre-stress was increased.

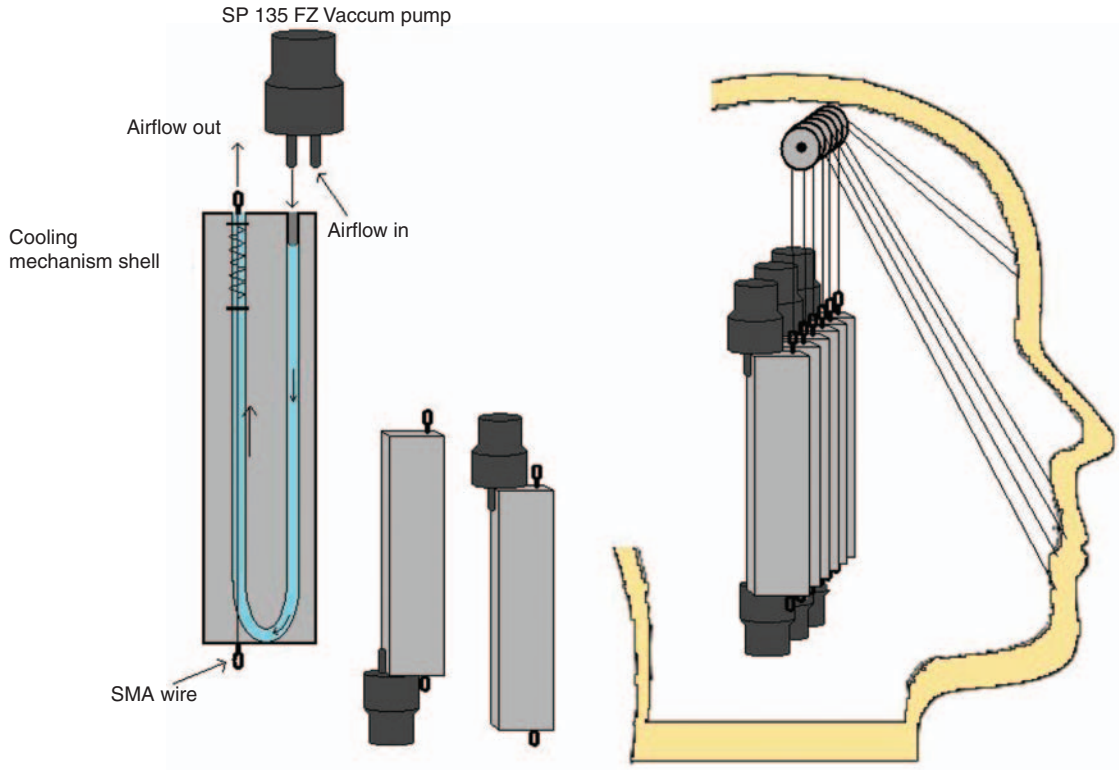

Figure 17. *Concept of a cooling mechanism in humanoid face that uses forced air cooling for creating deformation through contraction of SMA wires.*

For 100 μm diameter Flexinol wire, the force generation rate was of the order of 1–7 MPa/s in pre-stress range of 0–160 MPa whereas for 100 μm diameter Biometal fiber the force generation rate was 10–80 MPa/s in preload range of 0–320 MPa.

In order to further enhance the response time, active cooling of SMA wires was investigated. Active cooling technique based on thermal gel yielded 0% wire contraction due to excessive heat dissipation during the heating cycle. The active cooling technique based on flowing air reduced the response time by 35%. Heat sinking and forced air decreased the response time by 75% while fluid quenching decreased the response time by 87% (from 1.6 to 0.2 s). Flexinol was found to provide higher displacement and exhibited predictable behavior during cyclic actuations where Biometal fiber displayed a decaying performance due to stored energy within the wire. A concept has been proposed that uses forced air cooling coupled with biased springs for application of active cooling mechanism in a humanoid face. We hope that these experiments will advance the application of SMA into existing and new structures.

ACKNOWLEDGMENT

The authors gratefully acknowledge the financial support from office of Naval Research (ONR) through grant number N000140810654 and Institute of Critical research and Applied Science (ICTAS) at Virginia Tech.

REFERENCES

Akle, B.J., Bennett, M.D. and Leo, D.J. 2006. "High-strain Ionomeric–ionic Liquid Electroactive Actuators," *Sensors & Actuators: A: Physical*, 126:173–181.

Ashrafiuon, H., Eshraghi, M. and Elahinia, M.H. 2006. "Position Control of a Three-link Shape Memory Alloy Actuated Robot," *Journal of Intelligent Material Systems and Structures*, 17:381–392.

Baughman, R.H. 2005. "Playing Nature's Game with Artificial Muscles," *Science*, 308:63–65.

Bergamasco, M., Salsedo, F. and Dario, P. 1989. "A Linear SMA Motor as Direct-drive Robotic Actuator," In: *Proceedings of IEEE Conference on Robotics and Automation,* Vol. 1, pp. 618–623.

Bertacchini, O.W., Lagoudas, D.C., Calkins, F.T. and Mabe, J.H. 2008. "Thermomechanical Cyclic Loading and Fatigue Life Characterization of Nickel Rich NiTi Shape-memory Alloy Actuators," In: *Proceedings of SPIE*, Vol. 6929: 692916.

Boyd, J.G. and Lagoudas, D.C. 1994. "Thermomechanical Response of Shape Memory Composites," *Journal of Intelligent Material.Systems and Structures*, 5:333–346.

Choi, J.M., Son, H.M. and Lee, Y.J. 2008. "Design of Biomimetic Robot-eye System with Single Vari-focal Lens and Winding-type SMA Actuator," In: *International Conference on Control, Automation and Systems 2008*, 14–17 October, COEX, Seoul, Korea.

Hara, S., Zama, T., Takashima, W. and Kaneto, K. 2006. "Tris(trifluoromethylsulfonyl) methide-doped Polypyrrole as a Conducting Polymer Actuator with Large Electrochemical Strain," *Synthetic Metals*, 156:351–355.

Howe, R.D., Kontarinis, D.A. and Peine, W.J. 1995. "Shape Memory Alloy Actuator Controller Design for Tactile Displays", In: *Proceedings of IEEE Conference on Decision and Control, IEEE*, Vol. 4, pp. 3540–3544.

Huang, W. and Wong, Y.L. 1999. "Effects of Pre-strain on Transformation Temperature of NiTi Shape Memory Alloy," *Journal of Materials Science Letters*, 18:1797–1798.

Hunter, I.W., Lafontaine, S., Hollerbach, J.M. and Hunter, P.J. 1991. "Fast Reversible NiTi Fibers for Use in Microrobotics," In: *Proceedings of IEEE Conference on Micro Electro Mechanical Systems*, pp. 166–170.

Incropera, F.P., DeWitt, D.P., Bergman, T.L. and Lavine, A.S. 2007. *Fundamentals of Heat and Mass Transfer*, Hoboken, New Jersey.

Jayender, J., Patel, V., Nikumb, S. and Ostojic, M. 2005. "Modelling and Gain Scheduled Control of Shape Memory Alloy Actuators," In: *Proceedings of the 2005 IEEE Conference on Control Applications*, Toronto, Ontario.

Kornbluh, R., Perline, R., Eckerle, J. and Joseph, J. 1998. "Electrostrictive Polymer Artificial Muscle," In: *Proceedings of IEEE Conference on Robotics and Automation*, Vol. 3, pp. 2147–2154.

Kornbluh, R., Pelrine, R., Pei, Q., Oh, S. and Joseph, J. 2000. "Ultrahigh Strain response of Field-actuated Elastomeric Polymers," In: Bar-Cohen, Y. (ed.), *Proceedings of SPIE, Smart Structure and Materials, 2000: Electroactive Polymer Actuators and Devices (EAPAD)*, Vol. 3987, pp. 51–64.

Kumar, P.K., Lagoudas, D.C., Zanca, K.J. and Lagoudas, M.Z. 2006. "Thermomechanical Characterization of High Temperature SMA Actuators," In: Armstrong, W.D. (eds), *Proceedings of the SPIE, Smart Structures and Materials 2006: Active Materials: Behavior and Mechanics*, Vol. 6170, pp. 306–312.

Kusagawa, M., Nakamura, T. and Asada, Y. 2001. "Fundamental Deformation and Recovery Behaviors of Ni-Ti-Nb Shape Memory Alloy," *JSME International Journal Series A*, 44:57–63.

Lagoudas, D.C., Miller, D.A., Rong, L. and Kumar, P.K. 2009. "Thermomechanical Fatigue of Shape Memory Alloys," *Smart Materials and Structures*, 18:085021.

Leo, D.J. 2007. *Engineering Analysis of Smart Material Systems: Analysis, Design, and Control*, John Wiley and Sons, New York.

Li, Y., Cui, L., Shi, P. and Yang, D. 2001. "Phase Transformation Behaviors of Prestrained TiNi Shape Memory Alloy Fibers Under the Constraint of a Hard Substrate," *Materials Letters*, 49:224–227.

Loh, C.S., Yokoi, H. and Arai, T. 2005a. "Improving Heat Sinking in Ambient Environment for the Shape Memory Alloy (SMA)," In: *Proceedings of IEEE Conference on Intelligent. Robots and Systems*, pp. 3560–3565.

Loh, C.S., Yokoi, H. and Arai, T. 2005b. "New Shape Memory Alloy Actuator: Design and Application in the Prosthetic Hand," In: *Proceedings of the 27th Annual Conference of the IEEE Engineering in Medicine and Biology*, 1–4, September, Shanghai, China.

Lubliner, J. and Auricchio, F. 1996. "Generalized Plasticity and Shape Memory Alloys," *International Journal of Solids and Structures*, 33:991–1003.

Luo, Y., Takagi, T., Maruyama, S. and Yamada, M. 2000. "A Shape Memory Alloy Actuator using Peltier Modules and R-phase Transition," *Journal of Intelligent Material Systems and Structures*, 11:503–511.

Luchetti, T., Zanella, A., Biasiotto, M. and Saccagno, A. 2009. "Electrically Actuated Antiglare Rear-view Mirror Based on a Shape Memory Alloy Actuator," *Journal of Materials Engineering and Performance*, 18:717–724.

Madden, P.G.A., Madden, J.D.W., Anquetil, P.A., Vandesteeg, N.A. and Hunter, I.W. 2004. "The Relationship of Conducting Polymer Actuator Material Properties to Performance," *IEEE Journal of Oceanic Engineering*, 29:696–705.

McNichols, J.L. and Brooks, P.C. 1981. "NiTi Fatigue Behavior," *Journal of Applied Physics*, 52:7442–7444.

Moallem, M. and Tabrizi, V. 2009. "Tracking Control of an Antagonistic Shape Memory Alloy Actuator Pair," *IEEE Transactions on Control Systems Technology*, 17:184–190.

Nascimento, M.M.S.F. and Araujo, C.J. 2006. "Electro-thermomechanical Characterization of Ti-Ni Shape Memory Alloy Thin Wires," *Materials Research*, 9:15–19.

Oh, H.U., Izawa, K. and Taniwaki, S. 2005. "Development of Variable–damping Isolator using Bio-metal Fiber for Reaction Wheel Vibration Isolation," *Smart Materials And Structures*, 14:928–933.

Otsuka, K. and Wayman, C.M. 1999. *Shape Memory Materials*, Cambridge University Press, Cambridge, UK.

Patoor, E. and Berveiller, M. 1997. "Micromechanical Modelling of the Thermomechanical Behavior of Shape Memory Alloys," In: Berveiller, M. and Fischer, F.D. (eds), *Mechanics of Solids with Phase Changes*, pp. 121–188, Springer-Verlag, Wien, New York.

Pons, J.L., Reynaerts, D., Peirs, J., Ceres, R. and VanBrussel, H. 1997. "Comparison of Different Control Approaches to Drive SMA Actuators," In: *Proceedings of the IEEE Conference on Advanced Robotics*, pp. 819–824.

Qiu, J., Tani, J., Osanai, D., Urushiyama, Y. and Lewinnek, D. 2000. "High-speed Response of SMA Actuators," In: *Proceedings of International Journal of Applied Electromagnetics and Mechanics*, Vol. 12, pp. 87–100.

Reynaerts, D. and Van Brussel, H. 1991. "Development of a SMA High Performance Robotic Actuator," In: *Proceedings of the IEEE Conference on Advanced Robotics,* Vol. 1, pp. 61–66.

Russell, R.A. and Gorbert, R.B. 1995. "Improving the Response of SMA Actuators," In: *Proceedings of the IEEE Conference on Robotics and Automation*, Vol. 3, pp. 2299–2304.

Shaw, J.A. 2000. "Simulations of Localized Thermo-mechanical Behavior in a NiTi Shape Memory Alloy," *International Journal of Plasticity*, 16:541–562.

Shiraishi, Y., Yambe, T., Sekine, K., Saijo, Y., Wang, Q., Liu, H. et al 2005. "Development of an Artificial Myocardium Using a Covalent Shape-memory Alloy Fiber and its Cardiovascular Diagnostic Response," In: *Proceedings of the 27th Annual Conference of the IEEE Engineering in Medicine and Biology*, pp. 406–408.

Tadesse, Y., Priya, S., Stephanou, H., Popa, D. and Hanson, D. 2006. "Piezoelectric Actuation and Sensing for Facial Robotics," *Ferroelectrics*, 345(1):13–25.

Tadesse, Y. and Priya, S. 2008. "Humanoid Face Utilizing Rotary Actuator and Piezoelectric Sensors," In: *IMECE 2008: Mechanics of Solids, Structures and Fluids*, Vol. 12, pp. 573–581.

Tanaka, K., Nishimura, F. and Tobushi, H. 1994. "Phenomenological Analysis on Subloops in Shape Memory Alloys Due to Incomplete Transformations," *Journal of Intelligent Material.Systems and Structures*, 5(4):487–493.

Tobushi, H., Nakahara, T., Shimeno, Y. and Hashimoto, T. 2000. "Low-cycle Fatigue of TiNi Shape Memory Alloy and Formulation of Fatigue Life," *Transacations of ASME*, 122:186–191.

Villanueva, A., Bresser, S., Chung, S., Tadesse, Y. and Priya, S. 2009. "Jellyfish Inspired Underwater Unmanned Vehicle," In: *Proceedings of SPIE*, Vol. 7287, p. 72871G.

Wada, K. and Liu, Y. 2005. "Shape Recovery of NiTi Shape Memory Alloy under Various Pre-strain and Constraint Conditions," *Smart Materials and Structures*, 14:S273–S286.

Yan, X. and Nie, J. 2003. "Study of a New Application Form of Shape Memory Alloy Superelasticity," *Journal of Smart Materials and Structures*, 12:N14–N23.

Zhou, B. and Yoon, S.H. 2006. "A New Phase Transformation Constitutive Model of Shape Memory Alloys," *Journal of Smart Materials and Structures*, 15:1967–1973.